THE AEROGEOPHYSICAL ATLAS OF TOCANTINS STATE: SYNTHESIS OF MAGNETIC ANOMALY AND RADIOELEMENT MAPS WITH EMPHASIS ON REGIONAL SIGNATURES AND THE SERRA DA CANGALHA IMPACT STRUCTURE

Adolfo Barbosa da Silva [1,2*], Marcelo Ferreira da Silva [3],

Wolf Uwe Reimold [2], Felipe da Mota Alves [1], Alexandre Lisboa Lago [4],

Marco Antônio Couto Jr [5], Antônio Augusto S. Frasca [1], and Pedro Sérgio Estevam Ribeiro [1]

[1] Serviço Geológico do Brasil, Geological Survey of Brazil, Goiânia, GO, Brazil
[2] Universidade de Brasília, Postgraduate Program in Geology, Institute of Geosciences, Brasília, DF, Brazil
[3] Serviço Geológico do Brasil,Geological Survey of Brazil, Palmas, TO, Brazil
[4] Serviço Geológico do Brasil, Geological Survey of Brazil, Rio de Janeiro, RJ, Brazil
[5] Vale S/A, Nova Lima, MG, Brazil

*Corresponding author email: adolfo.barbosa@sgb.gov.br

ABSTRACT. The Tocantins State Aerogeophysical Atlas (TSAA) is an institutional product of the Geological Survey of Brazil. It is aimed at promoting the use of airborne magnetic and gamma-ray spectrometry data to support geophysical and geological research at state level. Here, we present a synthesis of the TSAA with special emphasis on the interpretation of the magnetic (Anomalous Magnetic Field, First Vertical Derivative (FVD), and Total Gradient Amplitude (TGA) images) and radiometric (RGB composite color map of concentrations, Inverse Images of K, eTh, and eU, and Normalized eU enhancement) map. In particular, the radiometric data for the Serra da Cangalha impact structure in northeast Tocantins are discussed. For Tocantins State, the results show that the radiometric and/or magnetic signatures of geological units (e.g., Mosquito Formation basalts; granite-gneiss/migmatite terrains) and structural features (e.g., dykes and lineaments), or related exogenous deposits (Serra Geral do Tocantins quartzose soils; alluvial deposits of main drainage channels) can be visualized well on regional-scale maps. Analysis of radiometric ratios for the area of the Serra da Cangalha impact structure indicates that eU concentrations are enriched in the annular basin around the central uplift structure, and in the zone straddling the contact between the Piauí and Pedra de Fogo formations. In the latter case, the elevated eU concentrations could be related to brecciated chert layers or silicified sandstones.

Keywords: Tocantins state aerogeophysical data; gamma-ray spectrometry; magnetometry; geological-geophysical integration; Serra da Cangalha impact structure

INTRODUCTION

In order to contribute to the improvement of geological knowledge and the discovery of mineral resources in Brazil, the federal government, through the Geological Survey of Brazil (GSB), has made important investments over the last two decades in acquisition of airborne geophysical data, such as airborne magnetics and gamma-ray spectrometry data acquisition (Pinto, 2022). An area of ca. 3,726,364 km² (or 92 % of the outcropping basement) of the Brazilian territory was covered by high-density airborne surveys, with a line spacing of 500 m and a flight height of 100 m (Oliveira and Rodrigues, 2019; Pinto, 2022).

With the aim to improve the dissemination of knowledge and the availability of aerogeophysical data to the technical-scientific community, the GSB has published a series of State Aerogeophysical Atlases (e.g., Pernambuco, Rondônia, Ceará, Goiás, Roraima, and others: Oliveira and Rodrigues, 2019; Graça and Silva, 2020; Sousa, 2021; Alves et al., 2022; Oliveira, 2022). In these atlases, airborne geophysical data are integrated and correlated with geology, according to Brazilian state limits. This compartmentalization is aimed at facilitating the management and use of the geophysical data according to the preferences and priorities of the public and/or private entities, and in relation to geological characteristics and local mineral potential. It is expected that the information contained in these atlases can help in the planning and execution of public policies, as well as decision-making, by private entities.

This article provides a synthesis of the Tocantins State Aerogeophysical Atlas (TSAA) as published by the GSB (Silva and Alves, 2021). In the TSAA, magnetic and gamma-ray spectrometry signatures were interpreted taking into account geological units that had been mapped in the state of Tocantins. Additionally, airborne geophysical data were used in three case studies, whereby the magnetic and/or gamma-ray spectrometry signatures of two known mineral deposits (the Palmeirópolis polymetallic and Alecrim/Campos Belos uranium deposits) and the Serra da Cangalha impact structure are analyzed in greater detail than before.

Some of the main interpretations of magnetic (Anomalous Magnetic Field and First Vertical Derivative and Total Gradient Amplitude) and radiometric (RGB color composite of concentrations and ratios) signature maps are emphasized. These maps were chosen because they are amongst the most common products used in geological-geophysical interpretation. From the selected case studies, only the radiometric signatures of the Serra da Cangalha impact structure are presented here. This work can contribute to a better understanding of airborne geophysics over Tocantins State and may encourage the development of new research approaches.

GEOLOGICAL SETTING

Geology of Tocantins State

A large portion of the Tocantins territory, namely the part not covered by consolidated and unconsolidated sediments, is composed of rocks of the Tocantins Province (Almeida et al., 1981) (Figure 1a). This geological province comprises three fold belts of Neoproterozoic age, which are known as the Araguaia, Paraguay, and Brasília Belt. The latter is located at the western margin of the São Francisco Craton (Figure 1a). There are also several other cratonic blocks (the Parnaíba, Paranapanema, and Goiás Massif), which were part of the amalgamation of western Gondwana (e.g., Brito Neves and Cordani, 1991; Pimentel and Fuck, 1992; Delgado et al., 2003; Mantovani and Brito Neves, 2009; Soares et al., 2018). The geotectonic compartmentalization of Tocantins State, as based on previous works (Pimentel et al., 2000; Frasca, 2015), can be summarized as follows: Archean-Paleoproterozoic TTG domes; basement of the Tocantins Structural Province; Paleoproterozoic Rift Basins (Araí, Serra da Mesa, and Natividade); remnants of Mesoproterozoic oceanic crust (Palmeirópolis Complex); Neoproterozoic orogens (Araguaia and Brasilia); Neoproterozoic passive margin basins (Paranoá Group) and platforms of the São Francisco Craton (Bambuí Group); the Paleozoic Parnaíba and Cretaceous (Urucuia Group) Sanfranciscana intracratonic basins, the Silurian-Devonian Água Bonita graben, and the Cenozoic Bananal sedimentary basin (Figure 1b).

The TTG domes (Colmeia, Lontra, Grota Rica, and Cocalancia) crop out in the northern part of Tocantins State and form the basement of the northern Araguaia Orogen (Figure 1b). These domes are correlated with rocks from the SW part of the Amazonian Craton (Moura and Gaudette, 1999). In the southern portion of the Araguaia orogen, basement is composed of ortho- and para-derived metamorphic rocks of the Porto Nacional and Rio dos Mangues complexes, and granites and cogenetic volcanic rocks of the Ipueiras Suite (Ribeiro and Alves, 2017) (Figure 1b). The southeastern portion of the basement in Tocantins State is represented by the Natividade-Cavalcante Block. This block is a Paleoproterozoic core that represents an extension of the São Francisco Paleocontinent. The block was deformed in the Brasiliano Orogeny (Fuck et al., 2014; Martins-Ferreira et al., 2020). This geotectonic unit is composed of greenstone belts (Riachão do Ouro Group), granite-gneiss (Almas-Cavalcante Complex), TTGs (Serra do Boqueirão Suite), and deformed granitic rocks (Aurumina Suite), and mafic-ultramafic intrusions (Frasca et al., 2010, 2018; Abdallah and Meneghini, 2017) (Figure 1b).

The basement in the southeastern Tocantins State is composed of geotectonic units that can be related to divergent tectonics (Figure 1b). These terranes comprise a Paleoproterozoic rift basin and remnants of Mesoproterozoic oceanic crust. The former involves metasedimentary and metavolcano-sedimentary sequences of the Araí, Serra da Mesa, and Natividade groups (Figure 1b). The latter is represented by metavolcano-sedimentary sequences of the Palmeirópolis Complex (Oliveira, 2000; Martins-Ferreira et al., 2018a, 2018b). This complex has considerable deposits of Cu, Pb, and Zn. The shales and graphite phyllites of the Água Suja Group and the Ticunzal Formation represent a portion of the Goiás Massif located in Tocantins State. This massif has been interpreted as an exotic and allochthonous continental block of a long and complex crustal evolution, which collided against the western margin of the San Francisco craton in the Neoproterozoic, during the final stages of the Brasiliano Orogeny (Jost et al., 2010, 2013).

In southern Tocantins State, a number of Paleo- to Mesoproterozoic granitic intrusions of the Tocantins River Stanniferous Subprovince have been mapped (Figure 1b). These bodies are in intrusive and tectonic contact with the host metasedimentary rocks of the Serra da Mesa and Araí groups (Marini and Botelho, 1986). The most prominent of these bodies of this subprovince is the Serra Dourada Granite. The strata of the Serra da Mesa Group are also intruded by syenites and monzonites that make up the Peixe Alkaline Suite (Frasca et al., 2018). Alkaline rocks (Monte Santo-Serra da Estrela Suite) also occur in the central-west portion of the state. It has been suggested that these rocks could have been associated with the beginning of fragmentation of the Rodinia supercontinent (Arcanjo et al., 2001). This episode triggered the formation of the "Araguaia Rift", with subsequent deposition of sediments into the precursor basin (Baixo Araguaia Group - Arcanjo et al., 2013).

The Baixo Araguaia Group is the main lithostratigraphic unit of the Araguaia orogen that constitutes a large geotectonic province of preferential N-S direction of more than 1,000 km length and 150 km width (Figure 1b). The Araguaia orogen is covered by Phanerozoic sedimentary rocks of the Parnaíba Basin to the north and east, and shows a tectonic relationship with afore-described Paleoproterozoic basement rocks. From base to top, the Baixo Araguaia Group is composed of the Morro do Campo, Xambioá, Canto da Vazante, Pequizeiro, and Couto Magalhães formations (Herz et al., 1989). Except for the Morro do Campo quartzites, the other formations are composed of pelitic rocks of varied metamorphic degrees (Gorayeb,

.

1981). The highest-grade metasedimentary rocks of the Baixo Araguaia Group host some granitic intrusions of syn- to late-orogenic origin, notably the Santa Luzia, Barrolândia, Presidente Kennedy, and Ramal do Lontra granites (Alves et al., 2019).

Serpentinized mafic-ultramafic bodies (Quatipuru Complex) also occur within Baixo Araguaia Group metasedimentary rocks (Paixão et al., 2008; Barros and Gorayeb, 2019). These bodies are believed to have been obducted during the agglomeration of West Gondwana, which would make the Araguaia Orogen a possible suture zone (Hodel et al., 2018). Metavolcano-sedimentary rocks of the Rio do Coco Group have been included in this complex as well (Maia de Souza et al., 2019). Thick, magnetite-rich dykes have been mapped in the Araguaia orogen (Hasui et al. 1980; Figueiredo et al., 2001).

Other Neoproterozoic tectonic units with prominent geophysical expressions in Tocantins State are the Goiás Magmatic Arc and the Brasilia orogen. The former is mainly represented by orthogneisses occurring in the central-southern part of Tocantins, and the latter comprises passive margin related metasedimentary and metavolcano-sedimentary rocks (e.g., Paranoá Group) that partially cover the basement in the southern part of Tocantins State (Marini et al., 1984; Fuck, 1994; Dardenne, 2000).
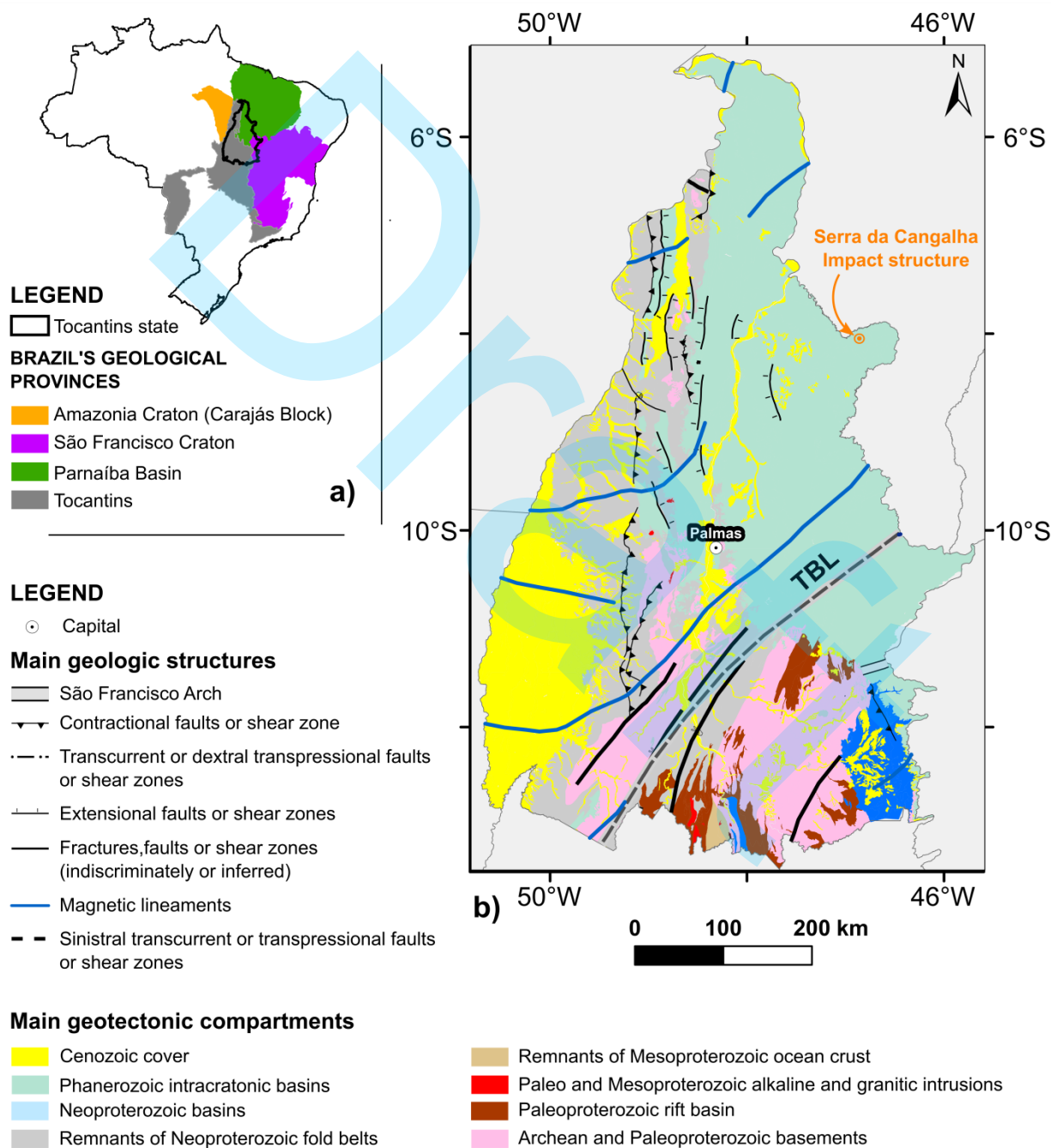

Figure 1: Simplified geology of Tocantins State. a) Position of the Tocantins State in relation to Brazil's geological provinces (after Santos, 2003). b) Simplified geotectonic compartment map for the state. TBL = Transbrasiliano Lineament. The main lithologies within these compartments are described in the text. The vectorial files of geological units were modified after Ribeiro et al. (2022).

In eastern Tocantins the extreme southeastern part of the sedimentary domain is composed of Neoproterozoic sequences of the Bambuí Group (Figure 1b). This includes several stratigraphic units such as diamictites, dolomites, clayey limestones, shale, siltstones, limestones, calcarenites, arkoses, quartz sandstones, and conglomerates (Martins-Neto et al., 2001; Alvarenga et al., 2007; Martins-Neto, 2009). The sedimentary domain in the eastern portion of the state is composed of sedimentary strata that were deposited in Phanerozoic intracratonic basins. Of these, the Parnaíba Basin is the largest, and its strata cover almost half of the state. The Parnaíba sedimentary column is predominantly siliciclastic, with subordinate limestone, anhydrite, and flint, in addition to injections of diabase and basalt that have been related to the Mosquito (Early Triassic) and Sardinha formations (Early Cretaceous), respectively (Góes and Feijó, 1994; Vaz et al., 2007; Oliveira et al., 2018). At the Tocantins and Bahia state border, Parnaíba Basin rocks are covered by eolian sandstones of the Posse and Serra das Araras formations (Campos and Dardenne, 1997a), which make up the Urucuia Group that, in turn, is part of the sedimentary succession of the Sanfranciscana Basin (Campos and Dardenne, 1997b; Sgarbi et al., 2001). Unconsolidated cover (Cenozoic Cover) rocks occur predominantly in the region bordering Pará State (Bananal Basin) (Figure 1b). These deposits essentially consist of alluvial sand, clay, and silt of the Araguaia Formation (Ribeiro and Alves, 2017). Such alluvial deposits, mainly sand and gravel, also occur along the Tocantins River. The Cenozoic cover also includes detrital crust formations (ferruginous laterite) that are distributed throughout the Tocantins territory (Sousa et al., 2012).

The structural framework within the limits of Tocantins State is essentially determined by the Transbrasiliano Lineament (TBL) (Schobbenhaus et al., 1975) (Figure 1b). The TBL has been interpreted as a transcontinental suture zone that is characterized by a system of NE-SW strike-slip faults stretching for more than 4000 km and extending as far as Africa and Argentina (Ramos et al., 2010, Cordani et al., 2013; Brito-Neves et al., 2014). The system shows evidence of predominantly dextral kinematics (Brito-Neves and Cordani, 1991; Brito-Neves et al., 2014).

The Serra da Cangalha impact structure

The Serra da Cangalha (SdC) structure in the northeasternmost part of Tocantins State (Figures 1b and 2a) is a 12 km diameter impact structure of complex morphology. It is located some 10 km from the small town of Campos Lindos, close to the border between Tocantins and Maranhão states (see Crósta et al., 2019, for a recent review) (Figure 2a and b). Since the 1970s, an impact origin had been suggested for SdC (Dietz and French, 1973; Reimold et al., 2006). However, robust evidence to support this hypothesis was only presented by Kenkmann et al. (2011) and Vasconcelos et al. (2013).
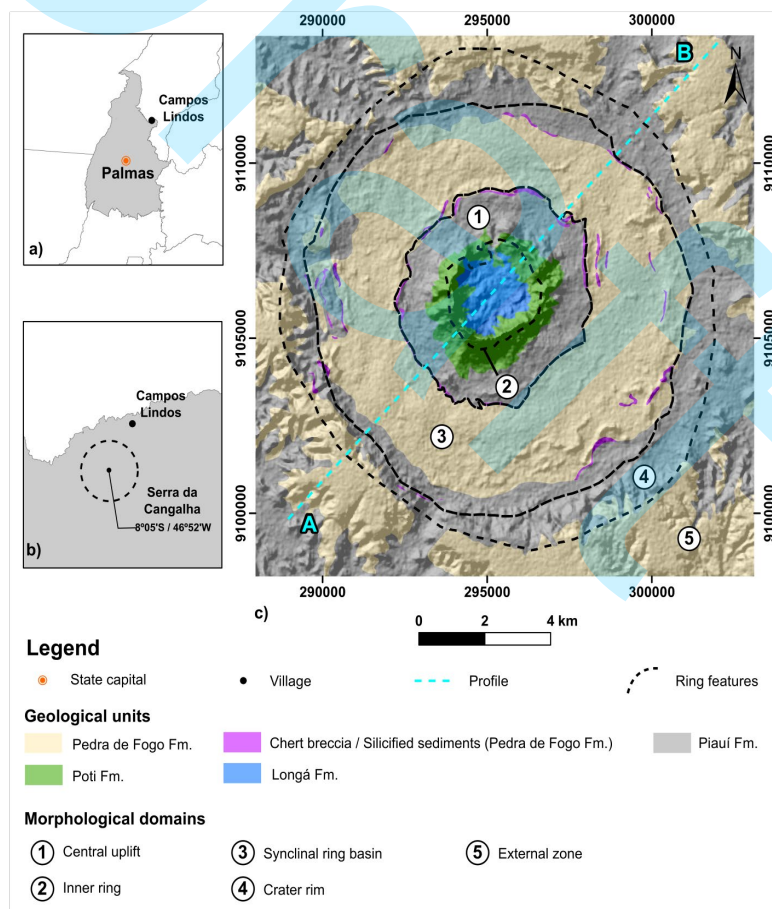

Figure 2: Survey area of the Serra da Cangalha (SdC) impact structure overlaid on elevation data (see Digital Elevation Model description in next section). The blue line corresponds to the A - B profile from which the radiometric ratios were extracted. a) Location of the town of Campos Lindos in relation to Palmas city, the capital of Tocantins state. b) Proximity between Campos Lindos and the SdC impact structure. c) Simplified geological map of the Serra da Cangalha (SdC) impact structure. Modified after Kenkmann et al. (2011) and Vasconcelos et al. (2013).

.

The SdC structure is entirely formed in sedimentary strata of the Parnaíba Basin. The local stratigraphic column involves, from base to top, shales, siltstones, and sandstones of the Longá and Poti formations (Mesodevonian Sequence – Eocarboniferous / Canindé Group) and sandstones, claystones, carbonates, and chert of the Piauí and Pedra de Fogo formations (Neocarboniferous – Early Triassic Sequence / Balsas Group) (Vaz et al., 2007; Kenkmann et al., 2011) (Figure 2c). The SdC morphology can be divided into four domains: central, annular basin; inner ring (collar of the central uplift); synclinal ring basin; and crater rim and external zone (Figure 2c) (Reimold et al., 2006; Kenkmann et al. 2011; Vasconcelos et al., 2013). It has been estimated that the structure has been significantly eroded since its formation, at least by some 500 m (Kenkmann et al., 2011). In the absence of datable impact-generated lithologies, the impact age has remained ill-defined. A maximum age is constrained only by the age of the youngest strata affected by the impact event. Thus, the age of the Pedra de Fogo Formation of ca. 250 Ma (Vaz et al., 2007) serves as the upper limit for the SdC impact age.

The central domain of the structure corresponds to a nearly circular region of 5.8 km diameter, which represents the central uplift complex of the structure (Figure 2c). This zone comprises an innermost depression where Longa Formation has been drilled. This depression is surrounded by a prominent collar of up to 300 m elevation and 3.4 km diameter (Reimold et al., 2006). This collar is composed of massive, strongly folded and silicified Poti Formation sandstones, and has given the name to this impact structure (Figure 2c). Impact-diagnostic shock metamorphic microdeformation features, shatter cones, and evidence of intense macrodeformation (folding, faulting) have been described from rocks of this central domain (Kenkmann et al., 2011; Crósta et al., 2019). The central domain can also be subdivided lithologically into three zones: an outer periphery – where red and sometimes white sandstones predominate, with fine to coarse granulometry, sub-rounded to rounded grains and moderate sorting; these rocks have been mapped as Piauí Formation; an inner collar that consists of a set of sub-vertical ridges formed by silicified sandstones of the Poti Formation; and the innermost depression of smooth topographic relief, where only very limited outcrop of medium- to coarse-grained sandstone, shale, and schist of the Longá Formation could be observed (Reimold et al., 2006; Vasconcelos et al., 2013). Locally, these innermost rocks have been found to contain shatter cones.

The Annular Basin domain is a topographically low region in which the main drainage channels occur (Reimold et al., 2006). Outcrops are scarce due to intense erosion and weathering. Such outcrops are, for the most part, formed by rocks of the Pedra de Fogo Formation, with additional subsidiary, local occurrences of rocks from the Piauí Formation. The main features of the annular basin domain are two sets of well-developed concentric ridges (Vasconcelos et al., 2013). The first set occurs at about 2.8 km from the center of the structure. It not only marks the Piauí Formation / Pedra de Fogo Formation contact zone, but also the outer margin of the central domain (central uplift structure). This first set is formed by brecciated chert layers and by silicified sandstones with minor claystone intercalations. The second set of chert ridges occurs at about 6 km from the center of the structure and involves deformed strata of the Pedra de Fogo Formation (Vasconcelos et al., 2013).

The crater rim domain marks the boundary of the SdC structure with the surrounding terrain (external domain). The crater rim is marked by a plateau with flat relief that is composed of rocks from the Pedra de Fogo Formation. The relatively flat external terrain shows very little evidence of deformation and is relatively flat. In this domain, Piauí Formation occurs at low altitude and the Pedra de Fogo Formation at comparatively higher stratigraphic and topographic levels (Vasconcelos et al., 2013). Kenkmann et al. (2011) provided a detailed description of the monocline structure that dips at moderate angles - along the inner slope of the crater rim - into the crater.

The principal domains of the SdC impact structure can also be recognized based on radiometric signatures, which was already proposed by Vasconcelos et al. (2012). In the innermost zone of the central domain (the inner depression), high K values were linked to high Al_2O_3 levels that suggested enhanced presence of muscovite in Longa Formation schist, whereas shales of the same formation would be related to high eU and eTh concentrations. On the other hand, products of erosion and weathering processes were implicated by those authors as main factors that could have contributed to comparatively low radiometric values observed over the area of the annular basin. Finally, the external zone is characterized by low K but high eU and eTh values, and this character could be related to the occurrence of lateritic soils (ibid).

METHODS

Processing of airborne geophysical data

The airborne geophysical data acquired over Tocantins State are derived from 6 aerogeophysical projects carried out by contracted companies between 2005 and 2016 (Figure 3). The main characteristic of these projects (e.g., spacing and direction of lines, sensors, interval sampling, preprocessing corrections) are given in Table 1 of the Supplementary Material. The average spacing of fight lines was 500 m and flight height was 100 m, for all projects.

The Oasis Montaj version 9.8.1 software was used to produce the Anomalous Magnetic Field (AMF) and the K, eTh and eU concentration grids. These grids were obtained from data interpolation by Bi-Directional (magnetic data) and Inverse Distance Weighted (radiometric data) methods with a 125 m cell size. Grid merging for the data sets of the different aerogeophysical projects was carried out using the Grid Knitting extension integrated into the Oasis software. The AMF grid was merged by using the suture method, whereas K, eTh, and eU concentration grids were merged by using the Blend method (Cheesman et al.,1998; Johnson et al., 1999).

From the AMF grid, the First Vertical Derivative of AMF (FVD-AMF) and Total Gradient Amplitude (TGA) were computed and the radioelement concentration grids were matched using the RGB composite color triangular system. These maps were chosen because they are the most commonly used ones in geological-geophysical interpretation (e.g., Airo 2002; Dentith and Mudge, 2014).
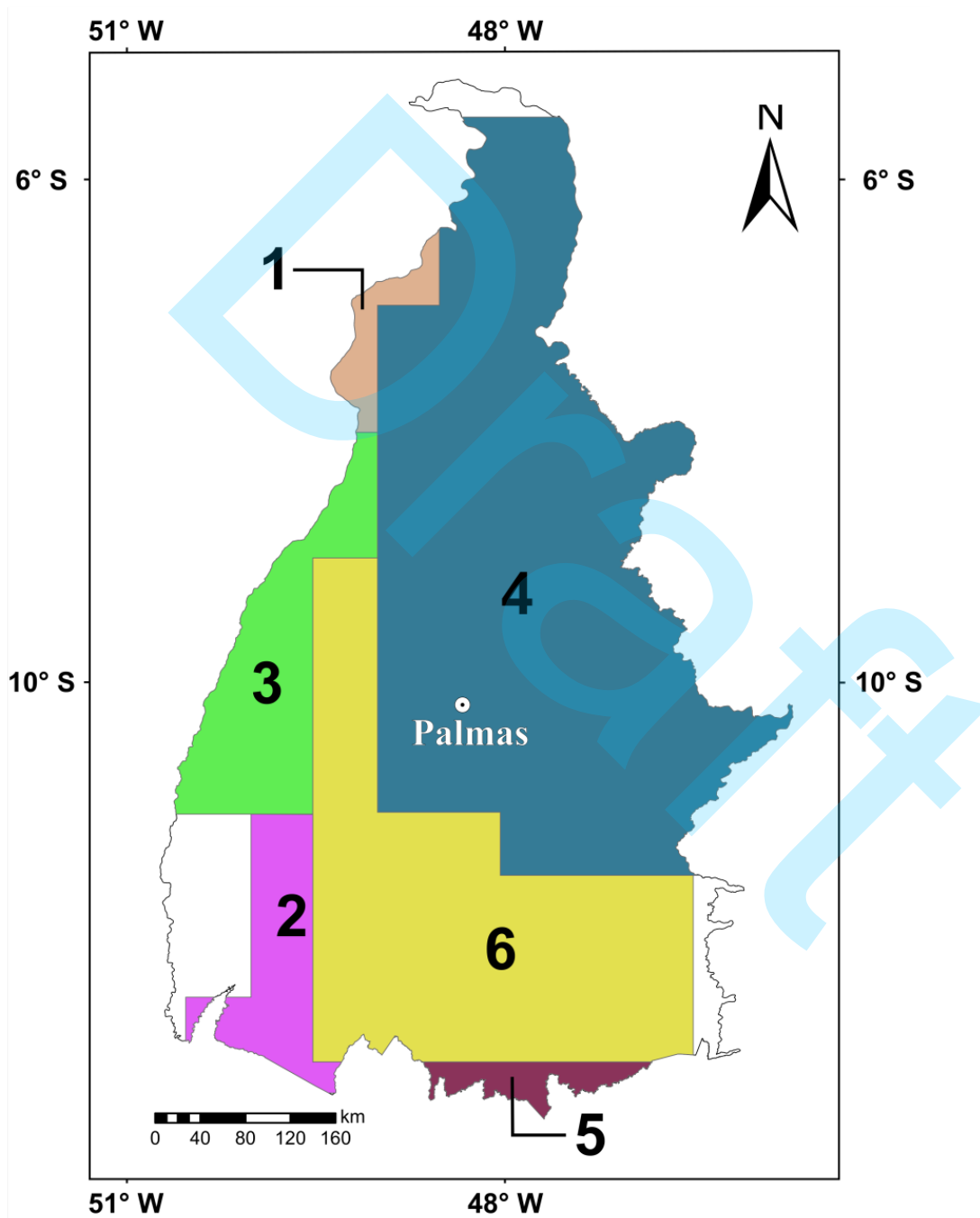

Figure 3: Aerogeophysical projects executed over Tocantins State. 1 – Rio Maria; 2 – Rio Formoso; 3 – Conceição do Araguaia; 4 – Parnaíba Basin; 5 – Tocantins Complement; 6 – Tocantins (compare the table in the Supplementary Material for further information about these projects).

The FVD-AMF is a type of transformation whereby the short wavelength magnetic signatures from shallow magnetic sources are enhanced, whilst the magnetic signal derived from deep sources is attenuated (Milligan and Gunn, 1997). For this reason, the FVD-AMF map is very useful in identifying and defining structural features generated by near-surface sources (e.g., Dentith and Mudge, 2014). The TGA – AMF, formerly known as Analytical Signal Amplitude (ASA) (Nabighian, 1972; Roest et al., 1992), is also a type of transformation that highlights the short wavelength magnetic signatures from shallow magnetic sources, but different from FVD, the TGA simplifies the magnetic anomaly shape, and, for 1D or 2D geometries, TGA centralizes the magnetic anomaly on causative bodies (Li, 2006). In this work, we follow the recommendation of previous studies (e.g. Reid, 2012; Li and Nabighian, 2015) and have decided to use the TGA nomenclature instead of the ASA terminology.

The RGB radioelement mapping facilitates the identification of areas relatively enriched/depleted in one or more elements by their respective, specific shades (Ford et al., 2008). Commonly, a RGB radioelement map is produced by placing the K grid into the red component (Red), the eTh grid into the green (Green), and the eU grid into the blue (Blue). Thus, bright shades denote areas enriched in the three radioelements, whereas dark areas denote relative depletion. Similarly, other RGB radioelement maps can be produced from the K, eTh, eU and their ratios. For instance, Duval (1983) proposed a RGB composite color scheme named Inverse Image of K, eTh, or eU. Such images match a given concentration grid of one element with their ratios in relation to the other two elements. For example: the K inverse image can be produced by placing the K grid into the red component (Red) and placing the K/eTh and K/eU ratio grids into the green (Green) and blue (Blue) components, respectively. In the K Inverse Image composition, areas with high K concentration and with K enrichment relative to eTh and eU are expected to be seen in bright tones, whereas dark areas denote low K concentration in conjunction with relative enrichment of eTh and eU to K (Duval 1983, Dentith and Mudge, 2014). The same idea can be expanded to get eTh or eU Inverse Images by matching eTh, eTh/eU, and eTh/K or eU, eU/K, and eU/eTh grids with RGB compositions, respectively.

For this work, we computed the radiometric ratios and produced K, eTh, and eU Inverse Image maps. In order to avoid that just one of the radioelements has a small spread of concentration estimates relative to its mean, which makes it difficult to see its contribution to the ratio map, we have normalized all radiometric grids before ratioing (Minty, 2011). This process was carried out to ensure that both radioelements in numerator and denominator can contribute equally to the enhancement of the differences between them across the study area (Minty, 2011).

In order to normalize the radiometric concentration, we use the MIN – MAX normalization according to this equation:

$$R_{norm} = \frac{R - Min_R}{Max_R - Min_R} \qquad (1)$$

where R is a radiometric variable (that is, K, eTh, or eU) and Min and Max are the minimum and maximum values of the radiometric variable. We verified that this does not change the distribution of radiometric concentrations significantly. When radiometric variables are normalized by equation (1), their values range from 0 to 1, and this ensures that both radioelements in the numerator and denominator can contribute equally to ratios. Moreover, possible negative values can also be suppressed, making the ratios more stable. Normalizing radiometric values has been essential for the method to highlight ratios (Minty, 2011) or as a pre-step for unsupervised clustering and machine learning methods (e.g., Pires de Lima and Marfurt, 2018; O´Leary et al., 2022). After normalizing the radioelements, we computed the ratios and produced the Inverse Images for K, eTh, and eU. It is worth mentioning that such Inverse Image maps were specially produced for this work and, therefore, they are not included in TSAA.

From visual analysis of magnetic, radiometric, and geological maps, some of the main aerogeophysical signatures were correlated with some of the geological units mapped in the territory of Tocantins State.

Processing of the airborne gamma-ray spectrometry data for the Serra da Cangalha impact structure

In order to facilitate the visualization of the correlation between the respective SdC domains and their radiometric signatures, a profile view of the radioelement concentration curves with a 3D view of the RGB map is superposed onto a digital terrain model (DEM). This DEM was derived from Shuttle Radar Topography Mission data acquired at 30 m resolution. Besides concentration curves of the main channels (K, eTh, and eU), eTh/K, eU/eTh, and eU/K ratio curves also were computed. The ratio curves highlight the differences in the geochemical behavior of the radioelements, thus allowing further interpretation (IAEA, 2003).

.

During the visual analysis of the profile of SdC radioelement curves, two points with relative eU enrichment were observed on the profile. In order to investigate the spatial context of this enrichment, we used the eU Inverse Image described in the previous subsection and a second map referred here as a normalized eU enhancement. This second map is an attempt to combine various elements into a single term to highlight one element of interest (Dentith and Mudge, 2014). Here, we used the eU/eTh and eU/K normalized ratios to derive the eU eU enhancement map by using the following equation:

$$NeU_E = \frac{eU}{eTh} \cdot \frac{eU}{K} = \frac{eU^2}{eTh \cdot K} \qquad (2)$$

where NeU_E is the normalized eU enhancement and K, eTh, and eU are normalized radiometric variables. Based on equation (2), areas with relative eU enrichment compared to eTh and K would be expected to have NeU_E high values. In the visual analysis, the geological map of SdC and the two points with eU enrichment seen in the profile were dropped onto the eU Inverse Image and the NeU_E.

RESULTS AND DISCUSSION

Significant correlations between airborne magnetic and radiometric data for the region of Tocantins State

In the Tocantins State Aerogeophysical Atlas (TSAA), results and discussion are presented in different sections dealing with correlations between main geological units and magnetic and gamma-ray spectrometry products. These correlations may suggest probable sources for the airborne geophysical signatures observed on the thematic maps. However, only dedicated studies of such possible sources can confirm, or not, the association between these proposed sources and the aerogeophysical signatures.

In this work, features whose magnetic and radiometric signals provide a regional expression have been analyzed. This form of analysis was chosen as such aerogeophysical signals can be easily visualized on regional maps, such as the magnetic and radiometric maps that are discussed here. Furthermore, although it is possible to identify several features on the regional maps, only 5 magnetic features (denoted M1 to M5 in Figures 4, 5, and 6) and 5 radiometric features (G1 to G5 in Fig. 7, 8, and 9) will be described and related to geological information. Because the eU Inverse Image yields a noisy representation of Tocantins State, we decided to show it only for the SdC impact structure in the next subsection. Finally, it is important to underline that magnetic and/or radiometric signals of chosen features can be related to one or more lithostratigraphic unit(s).

The features in areas M1 and G1 show that most of the granitic/gneissic/migmatite rocks that make up the Natividade-Cavalcante Block correlate with magnetic lows (low values on the AMF, FVD-AMF, and TGA - AMF maps) (Figs. 4, 5, and 6) and high radioelement abundances, mainly of K, which gives a reddish hue in the RGB radiometric concentration map (Figure 7) and a bright hue in the K Inverse Image (Figure 8). Comparing the Inverse Images (Figs. 8 and 9), it seems that the K Inverse Image yields better results in order to define the contours of granitic/gneissic/migmatite rocks, whereas the eTh Inverse Image shows such contours in a more diffuse way. As these terrains were affected by several types of metamorphism, it is possible that magnetite alteration and deformation could have contributed to the formation of the observed low magnetism (Airo 2002; Clark, 1997; Reeves, 2005). On the other hand, the radiometric pattern observed over these terrains may be associated with compositional aspects, as the rocks of the Almas-Cavalcante Complex and the Aurominas Suite are commonly enriched in radioelements, mainly in K (Alvarenga et al., 2007).

Among the magnetic signatures in the M1 area there is a set of short wavelength magnetic anomalies (indicated by white arrows in Figs. 4, 5, and 6) close to the Natividade-Cavalcante granitic/gneiss/migmatite rocks. Many of these anomalies appear to coincide with dark areas in the three RGB radiometric maps (RGB concentrations and K and eTh Inverse Images) (Fig. 7, 8, and 9). This is suggestive of low concentrations of K, eTh and eU (white arrows in Figure 7).
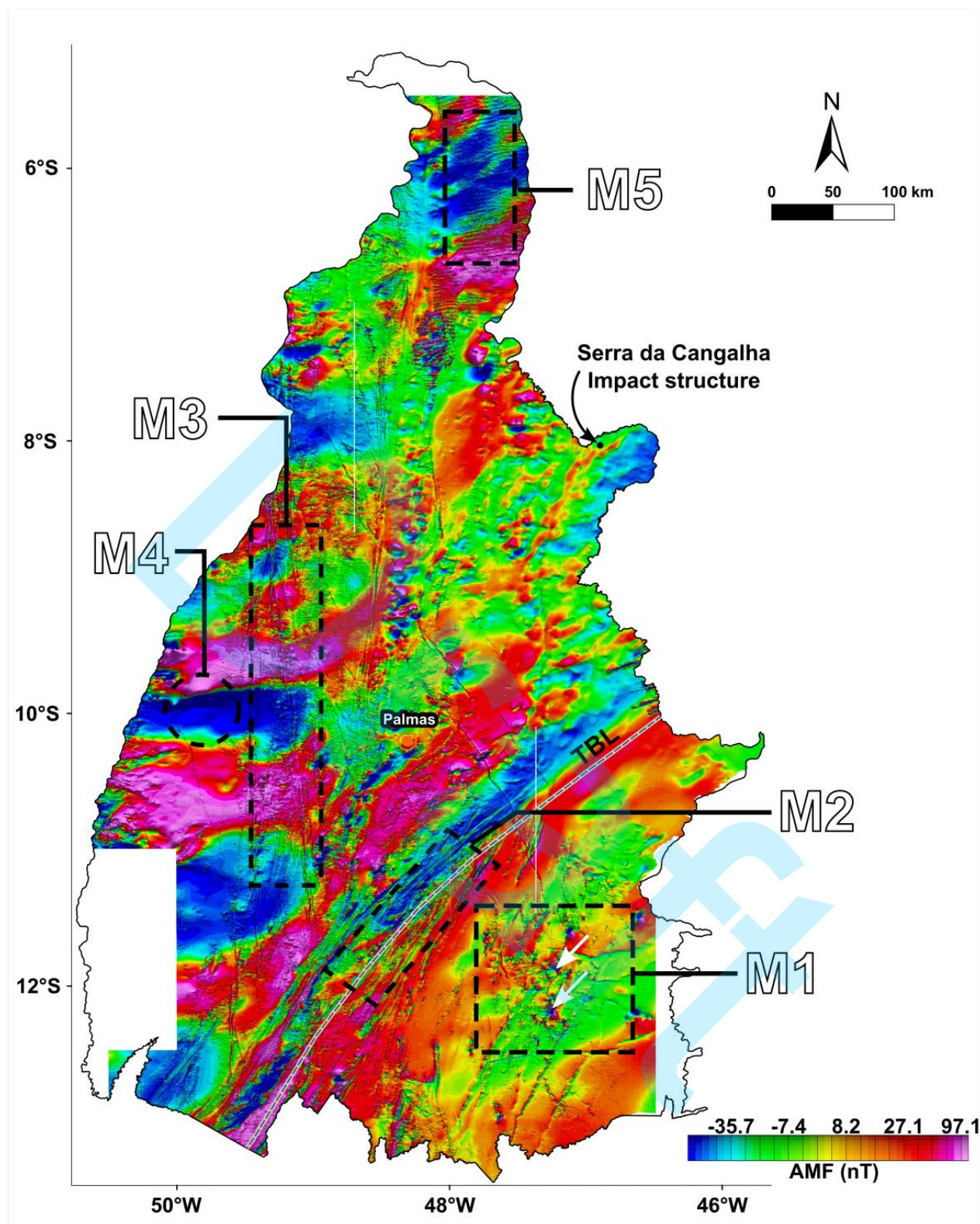
Figure 4: Anomalous Magnetic Field (AMF) map of Tocantins State. M1 – M5 correspond to features whose magnetic signatures can be visualized at regional scales. M1 - magnetic lows of granitic/gneiss/migmatite rocks. The white arrows highlight high-amplitude magnetic anomalies related to the Corrego do Paiol Formation metavolcanics or the Barra do Gameleira mafic intrusions; M2 - linear magnetic anomalies associated to the Transbrasiliano Lineament (TBL); M3 - linear magnetic anomalies associated with dikes and ophiolitic bodies; M4 - unknown circular magnetic anomaly. M5 – Magnetic signatures associated with Mosquito Formation basalts.
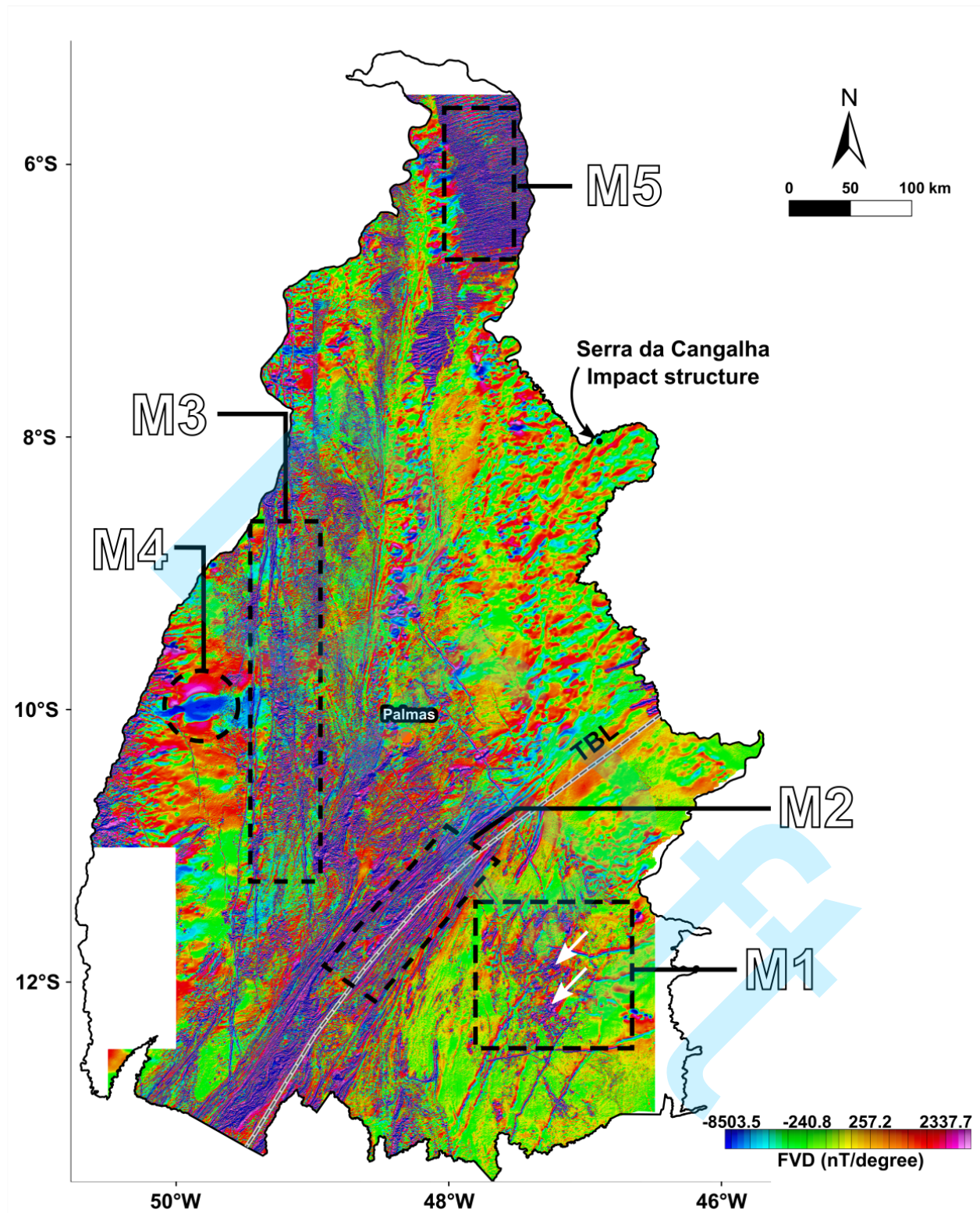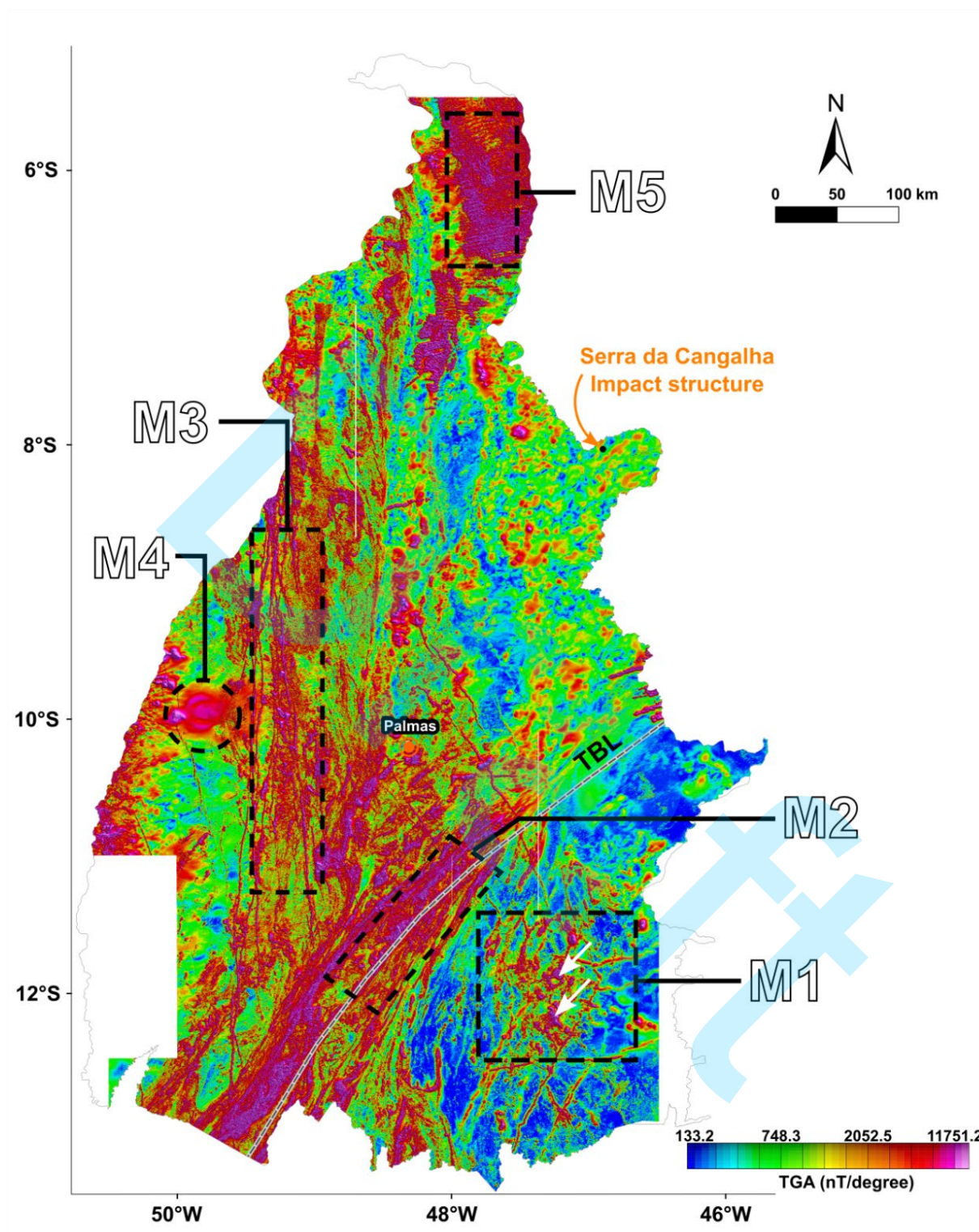
Figure 5: First Vertical Derivative of the Anomalous Magnetic Field (FVD – AMF) map of Tocantins State. M1 – M5 correspond to features whose magnetic signatures can be visualized at regional scales. M1 - magnetic lows of granitic/gneiss/migmatite rocks. The white arrows highlight high-amplitude magnetic anomalies related to the Corrego do Paiol Formation metavolcanics or the Barra do Gameleira mafic intrusions; M2 - linear magnetic anomalies associated with the Transbrasiliano Lineament (TBL); M3 - linear magnetic anomalies associated with dikes and ophiolitic bodies; M4 - sunknown circular magnetic anomaly. M5 – Magnetic signatures associated with Mosquito Formation basalts.

Figure 6: Total Gradient Amplitude of the Anomalous Magnetic Field (TGA – AMF) map of Tocantins State. M1 – M5 correspond to features whose magnetic signatures can be visualized at regional scales. M1 - magnetic lows of granitic/gneiss/migmatite rocks. The white arrows highlight high-amplitude magnetic anomalies related to the Corrego do Paiol Formation metavolcanics or the Barra do Gameleira mafic intrusions; M2 - linear magnetic anomalies associated with the Transbrasiliano Lineament (TBL); M3 - linear magnetic anomalies associated with dikes and ophiolitic bodies; M4 - unknown circular magnetic anomaly.

The zones of strong magnetization within the Natividade-Cavalcante Block may be associated with ferrimagnetic minerals in volcanosedimentary units, such as the metavolcanics of the Corrego do Paiol Formation at the base of the Riachão Group, the suite of Barra do Gameleira mafic intrusions, or even in Cretaceous mafic dykes (Sabóia and Meneghini, 2019; Martins-Ferreira et al., 2020). The low concentration of these radioelements in such rocks may also be a plausible explanation for the radiometric signatures observed as dark areas in the G1 region of Figures 7, 8, and 9 (Galbraith and Saunders, 1983; Airo, 2002).

The maps for areas M2 and G2 (compare Figures 4, 5, 6 and 7, 8, and 9) show a set of magnetic anomalies and radiometric patterns with linear shapes. The spatial locations of M2 and G2 signatures suggest that they could be related to the lithostratigraphic units that were affected by the Transbrasiliano Lineament. The cause of these magnetic anomalies and radioelement concentrations could be related to several factors, such as the juxtaposition of lithologies with contents of ferrimagnetic minerals and radioisotopes, and the deposition and accumulation of such minerals in fault troughs (Henkel and Guzmán, 1977; Airo, 2002). Similarly, magnetic signatures in area M3 (Figs. 4, 5, and 6) indicate linear shapes of great extensions. Such linear magnetic anomalies are well defined in FVD – AMF and TGA – AMF maps, suggesting that such anomalies come from near-surface sources. As has been suggested by Cruz and Gorayeb (2020), many of these anomalies may have been generated by mafic dykes, but others could also be due to the juxtaposition of units in thrust zones or along faults, or they could represent slivers of oceanic crust (ophiolites) (Paixão et al., 2008).

Weak radioelement concentrations also occur over the sedimentary domain. Such radiometric signatures are represented by the character of areas G3 and G4 (Figures 7, 8, and 9). In the former case, such low concentration areas may be due to the low natural concentrations of K, eTh and eU in Mosquito Formation basalts. The magnetic minerals in the subvolcanic lithotypes of this unit may be one of the main sources of high-intensity magnetic anomalies observed on magnetic anomaly maps, mainly on FVD – AMD and TGA – AMF maps, where such high-intensity magnetic anomalies show a linear, E-W directed pattern (Mocitaiba et al., 2017) (area M5 in Figures 4, 5, and 6). In the latter case of G4, low K, eTh, and eU concentrations may be associated with quartz-rich soils in the Serra Geral do Tocantins region (Silva and Alves, 2022). Residual landforms are represented in green and cyan (Fig. 7), and show that weathering may have favored eTh and eU concentrations and K leaching (Taylor et al., 2002; Mello et al, 2021). This idea is corroborated by K and eTh Inverse Images: the residual landforms show strong dark hues in K image inverse (G4 in Fig. 8), suggesting K leaching, whereas these same residual landforms can be seen as strong bright areas in the eTh Inverse Image (G4 in Fig. 9), which suggests eTh concentration. These results suggest that K and eTh Inverse Images can be a useful tool in highlighting products of weathering.
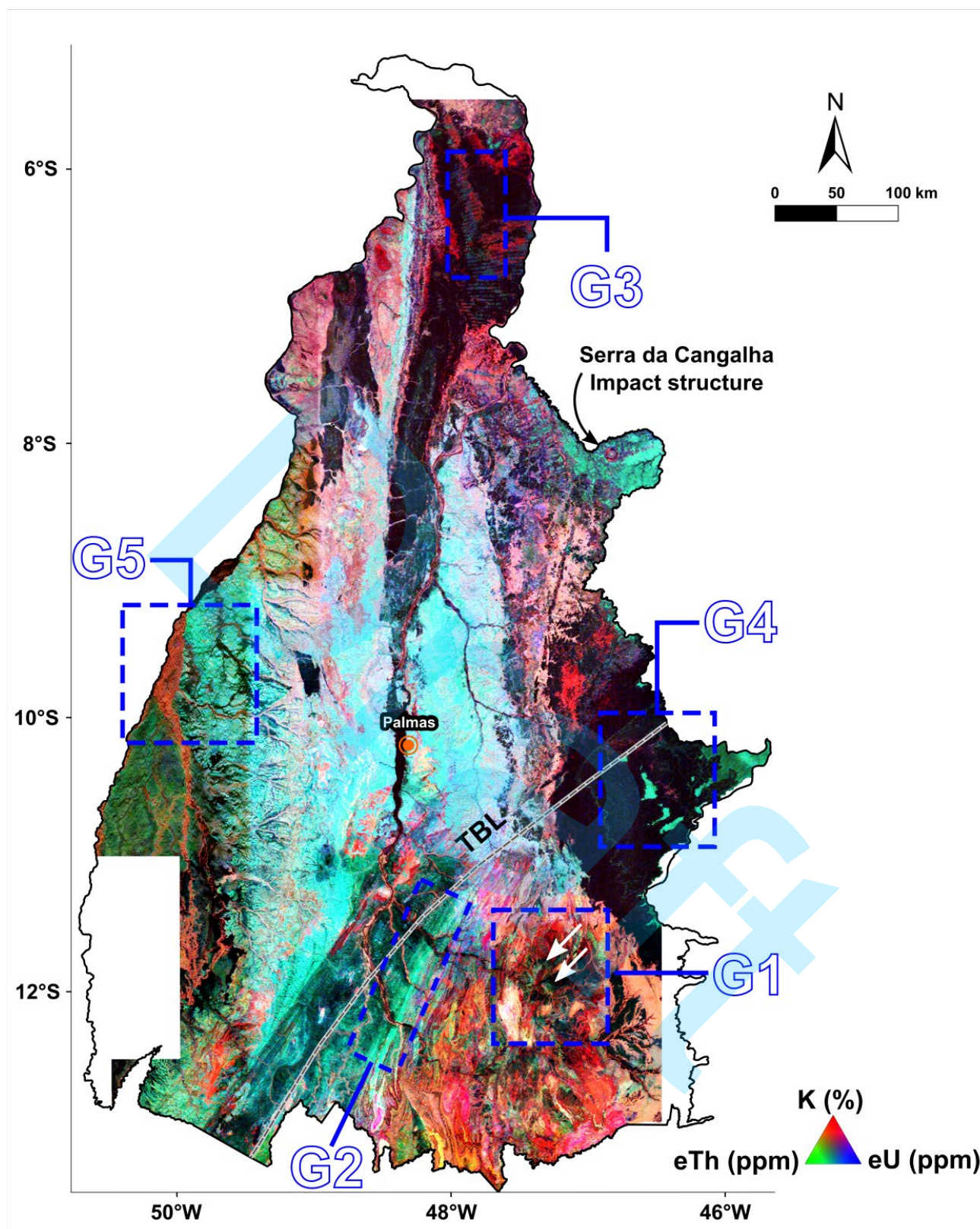
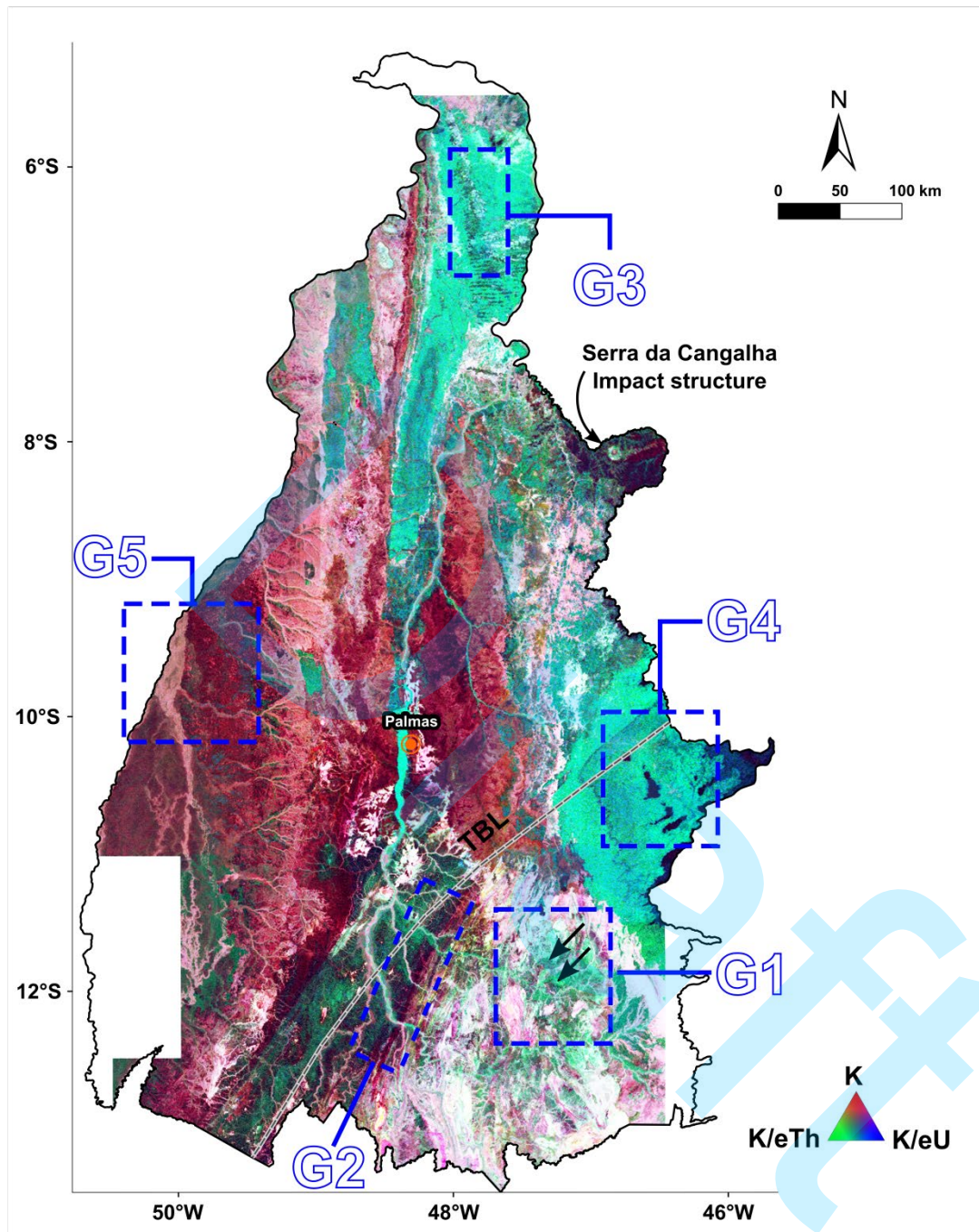Figure 7: RGB composite color map of the K, eTh, and eU concentrations over the territory of Tocantins State. Areas G1 – G5 correspond to features whose radiometric signatures can be distinguished at the regional scale. G1 - radiometric signatures of granitic/gneiss/migmatite terrain. The write arrows highlight low radiometric anomalies associated with mafic intrusions within these terrains; G2 - linear radiometric signatures associated with the Transbrasiliano Lineament (TBL); G3 - low radiometric anomaly due to the presence of Mosquito Formation basalts; G4 - low K, eTh, and eU concentrations associated with quartz-rich soils in the Serra Geral do Tocantins region. The residual landforms show comparatively enhanced eTh and eU concentrations; G5 - radiometric signatures of alluvial deposits.
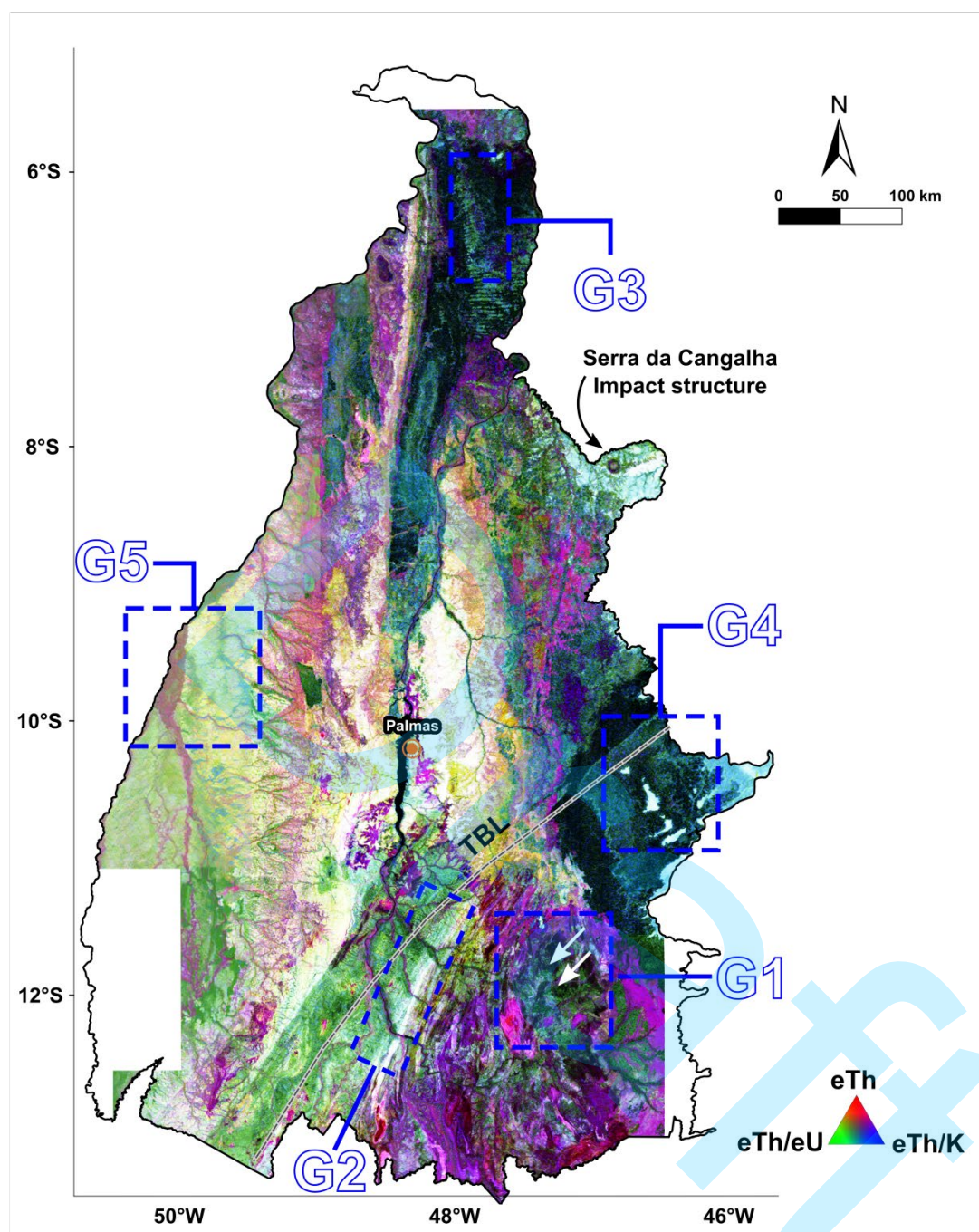
Figure 8: Potassium Inverse Image over the territory of Tocantins State. Areas G1 – G5 correspond to features whose radiometric signatures can be distinguished at the regional scale. G1 - radiometric signatures of granitic/gneiss/migmatite terrains. The black arrows highlight low radiometric anomalies associated with mafic intrusions within these terrains; G2 - linear radiometric signatures associated with the Transbrasiliano Lineament (TBL); G3 - low radiometric anomaly due to the presence of Mosquito Formation basalts; G4 - low K, eTh, and eU concentrations associated with quartz-rich soils in the Serra Geral do Tocantins region. The residual landforms show comparatively enhanced eTh and eU concentrations; G5 - radiometric signatures of alluvial deposits.

Figure 9: The eTh Inverse Image over the territory of Tocantins State. Areas G1 – G5 correspond to features whose radiometric signatures can be distinguished at the regional scale. G1 - radiometric signatures of granitic/gneiss/migmatite terrains. The black arrows highlight low radiometric anomalies associated with mafic intrusions within these terrains; G2 - linear radiometric signatures associated with the Transbrasiliano Lineament (TBL); G3 - low radiometric anomaly due to the presence of Mosquito Formation basalts; G4 - low K, eTh, and eU concentrations associated with quartz-rich soils in the Serra Geral do Tocantins region. The residual landforms show comparatively enhanced eTh and eU concentrations; G5 - radiometric signatures of alluvial deposits.

Radiometric signatures seen along large drainage channels, mainly along the Tocantins and Araguaia rivers and their tributaries, are also emphasized on the RGB maps (G5 area in Figures 7, 8, and 9). In western Tocantins (area G5), such anomalies may be derived from alluvial deposits (Bierwirth, 1996). In this case, the color distribution in Figure 7 (area G5) can provide clues about the composition or texture of these deposits. A white color suggests that such deposits are enriched in all 3 radioelements. It can, therefore, be inferred that either these deposits are recent or that their source is close to the place of deposition (Pickup and Marks, 2000; Wilford and Minty, 2007; Rawlins and Webster, 2007; Dent et al., 2013). On the other hand, a dark color suggests that such deposits are depleted in K, eTh and eU, which may imply that they are dominated by silica-rich minerals, mainly in the sand fraction (Spadoni and Voltaggio, 2013; Mello et al.,

2021). Regarding Inverse Images, the path of drainage channels is well-defined in the eTh Inverse Image because there are better contrasts between alluvial deposits and surrounding lithologies (Figure 9).

In the western State of Tocantins, radiometric signatures in the G5 area coincide with a somewhat smooth magnetic relief related to short-wavelength linear magnetic anomalies. However, a large (ca. 32 km wide) magnetic anomaly with an approximately circular shape (area M4 in Figs. 4, 5, and 6) seems to be associated with a deep magnetic source, as the magnetic signal is attenuated in the FVD – AMF and TGA maps (Figs. 5 and 6). This large circular magnetic anomaly is disturbed by some, previously mentioned, linear magnetic anomalies. The source of this circular magnetic anomaly is unknown, but the existence of circular magnetic anomalies in sedimentary basins may be indicative of mafic intrusions (Gunn, 1997). Alternatively, they may represent the location of a buried impact structure (Pilkington and Grieve, 1992; Gilder et al., 2018).

Radiometric signatures of the Serra da Cangalha impact structure

In the RGB maps (Figs. 7, 8, and 9) the radiometric signatures in the area of the SdC impact structure present a circular pattern. Such patterns have been observed for other impact structures (e.g., the Lawn Hill, Mount Toondina, Riachão Ring, and Araguainha impact structures)(Maziviero et al., 2013; Niang et al., 2022; Leite et al., 2022), and could be the outcome of a number of factors or processes, such as impact-induced K volatilization, impact melt differentiation, hydrothermal alteration, structural deformation, post-impact alteration, and distribution of ejecta deposits (Vasconcelos et al., 2012; Baratoux et al., 2019; Niang et al., 2021, 2022). In previous work about the SdC impact structure, it was suggested that the radiometric signatures there could be related to post-impact alteration, mainly to differential erosion of different lithostratigraphic units (Kenkmann et al 2011; Vasconcelos et al., 2012, 2013).

Here, we corroborate the results of this previous work with new imagery and observations. We observe an association between the main morphological domains of the SdC impact structure and their radiometric signatures. High K values occur in the area of the central depression, and low radiometric values are observed over the area of the annular basin. Outside of the crater rim, we also observe low K values and high eU and eTh values.

New information about the distribution and behavior of radioelements can be extracted from the analysis of radiometric ratio curves across the Serra da Cangalha structure. Figure 10 shows that the innermost depression in the central uplift domain of the structure is indeed characterized by high values of K, eTh, and eU, as already observed by Vasconcelos et al. (2012). However, the low values for the eTh/K and eU/K ratio curves over this centralmost area suggest enrichment of K. The K, eTh, and eU values in the central part of the annular basin are low, but eU/eTh and eU/K ratio values suggest that eU is enriched in this zone relative to K and eTh.

The low eTh/K and eU/K ratio over the inner part of the central domain can be explained not only by the presence of muscovite, as previously proposed by Vasconcelos et al. (2012), but also by the presence of alluvium containing K-bearing minerals derived from the erosion of the inner walls of the very prominent collar. In the context of impact structures, high K values have been observed to be sometimes correlated with topographic depressions filled by alluvial deposits (e.g., Niang et al., 2021). Similarly, high eTh and eU concentrations in the inner depression may be associated with Longa Formation shales (Vasconcelos et al, 2012). Furthermore, the presence of accessory minerals derived from erosion of the inner collar should not be ruled out as another possible carrier of radiogenic elements (eU and eTh).

Contrary to the central depression, the annular basin is characterized by low values for the radioelements. Erosion and weathering processes were proposed to explain the radiometric low observed over the annular basin (Vasconcelos et al., 2013). In areas where erosion processes are dominant, the radiometric response may be primarily associated with bedrock minerals or minerals derived from secondary processes (e.g., hydrothermal alteration or weathering) (Dickson and Scott, 1997). In places where weathering processes are dominant, high concentrations of eTh can be expected, as Th has a low mobility and, when released, is quickly incorporated into iron oxides or phyllosilicates. In addition, many weathering-resistant minerals are Th-rich (such as monazite, zircon, and iron oxides; Dickson and Scott, 1997; Wilford and Minty, 2007; Mello et al., 2021).

In Figure 10, the increments for the annular basin along the eU/eTh and eU/K ratio curves suggest that the annular basin is characterized by generally low K, eTh, and eU abundances. If weathering were one of the causes of this radiometric low, an enrichment of eTh relative to eU (that is, decrease along the eU/eTh curves) would be expected, similar to what has been observed over the crater rim zone (see discussion below). Therefore, if weathering contributed to the radiometric pattern observed over the annular basin, this contribution could be dominant. On the other hand, the low overall radiometric signature could be related to a lithostratigraphic unit that has been exposed by erosion. This unit could be low in K, eTh, and eU but could contain U-bearing minerals (e.g., zircon
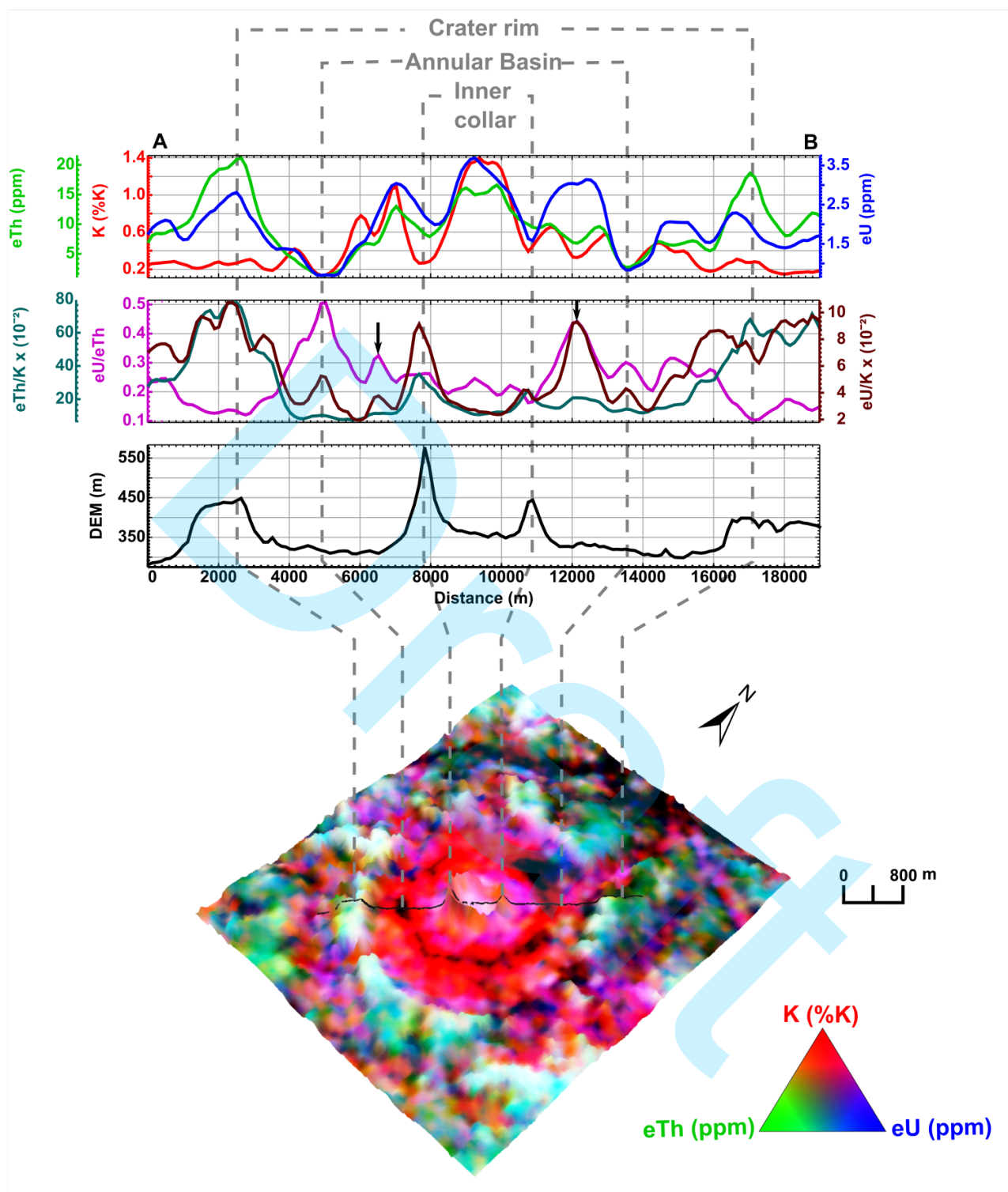
Figure 10: Profile A – B in SW – NE direction (compare Figure 2) is matched with a 3D visualization of the Serra da Cangalha impact structure based on the RGB composition of radiometric concentrations overlain onto a SRTM digital elevation model. Vertical exaggeration = 5x horizontal scale. The black arrows highlight areas where eU is relatively enriched compared to K and eTh, in the inner zone of the annular basin.

from aeolian sandstone). These increments along the eU/eTh and eU/K ratio curves could also be related to intermittent U anomalies, that is, the gamma rays detected during the aerial survey may come from Rn in groundwater discharge zones (Bierwirth, 1996; Wilfort et al., 1997). This is a potentially valid observation, as the annular basin is a focus of

drainage channels. It is, thus, recommended to carry out further studies aimed at elucidating the origin of this relative enrichment of eU in the annular basin at SdC. Such studies could include gamma-ray ground surveys, soil sampling for geochemical analysis, and petrographic descriptions. Multivariate analysis techniques (e.g., Principal Component Analysis, unsupervised clustering, correlation heatmaps) (Ford et al., 2008; Mello et al., 2021) could be applied to such data sets to identify the main contributors to U concentration. Additionally, in situ Rn measurements may be useful to investigate U concentrations derived from groundwater flows.

An interesting aspect of Figure 10 relates to the eU concentrations that are observed at the interface between the outer walls of the inner collar and the center of the annular basin, and which have not been discussed in earlier work. In the NE portion of the profile, at position 12,200 m, an increase in eU concentration is accompanied by a decrease in eTh and K concentrations. This behavior of the radiometric elements is well expressed along the eU/eTh and eU/K ratio curves. Within the region delimited by the inner collar and the center of the annular basin, it is possible to identify areas with local positive maxima on the eU/eTh and eU/K ratio curves, as indicated by black arrows in Figure 10, both to the SW and NE of the central part of the structure. In Figure 10 the center of the SdC structure is located approximately at position 9,400 m. Consequently, the distance between the peaks and the center of the structure is approximately 2,900 m (SW portion) and 2,800 m (NE portion). Interestingly, these distances are similar to those distances (2.8 km) from the center to where the first set of chert ridges occurs. These ridges mark the contact zone between the Piauí Formation and the Pedra de Fogo Formation, and they also mark the outer limit of the central uplift domain.

When the local positive maxima on the eU/eTh and eU/K ratio curves are plotted as a point in eU inverse image and NeU_E maps (Figs. 11 and 12), the northeasternmost point on profile coincides with Piaui and Pedra de Fogo contact zones and with high NeU_E values (see the white stars in Figs. 11 and 12). Otherwise, the southwesternmost point on the profile neither shows high NeU_E nor association with any contact zones. On the one hand, this result suggests that such lithostratigraphic contact zones present relative enrichment of eU and relative depletion of eTh and K abundances, such that we can infer that the eU concentrations could stem from brecciated chert layers or silicified sandstones. On the other hand, the final word about this enrichment has not yet been spoken and more researches must be done.
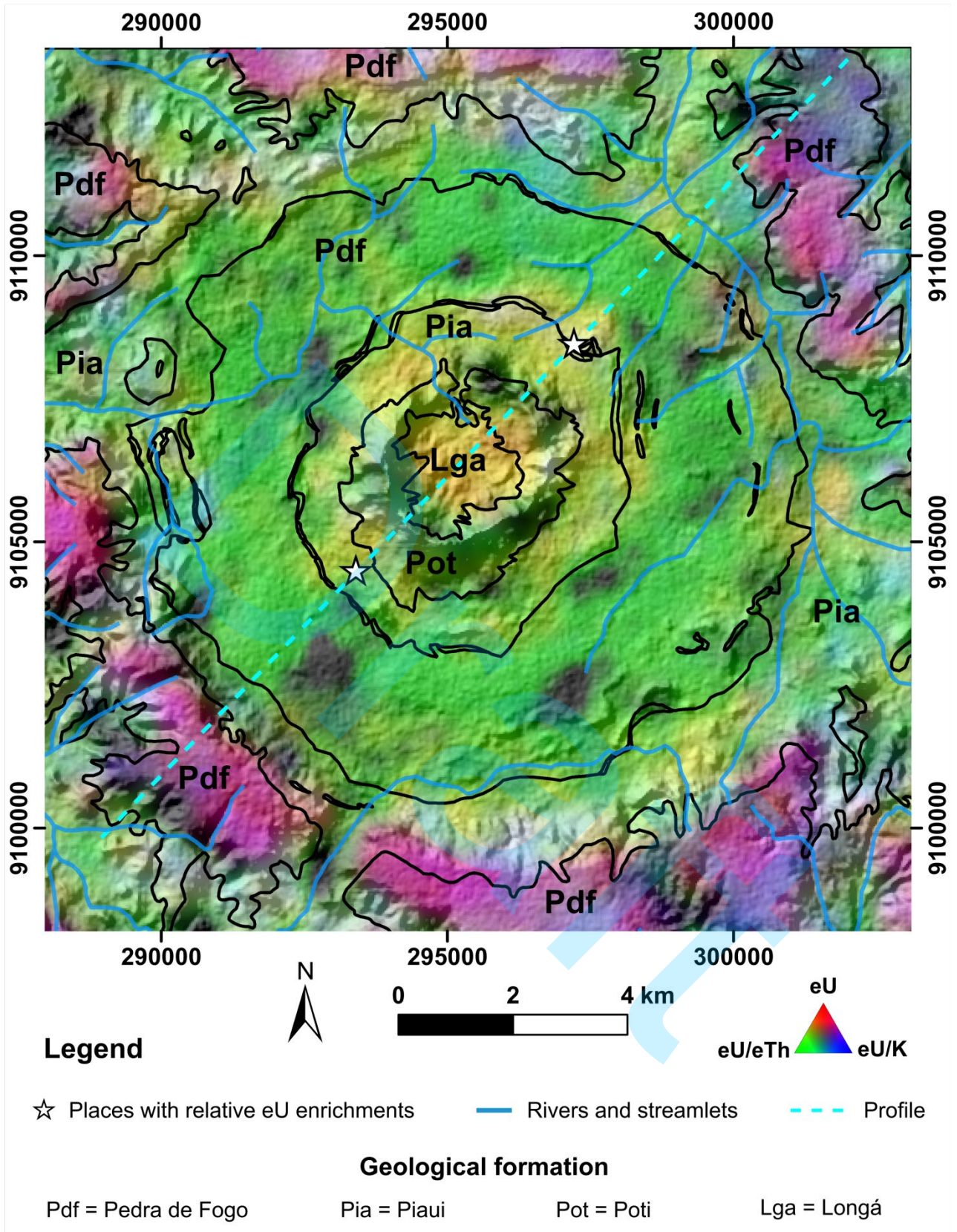
Figure 11: eU Inverse Image map of Serra da Cangalha impact structure. The white stars highlight areas where eU is relatively enriched compared to K and eTh, in the inner zone of the annular basin.
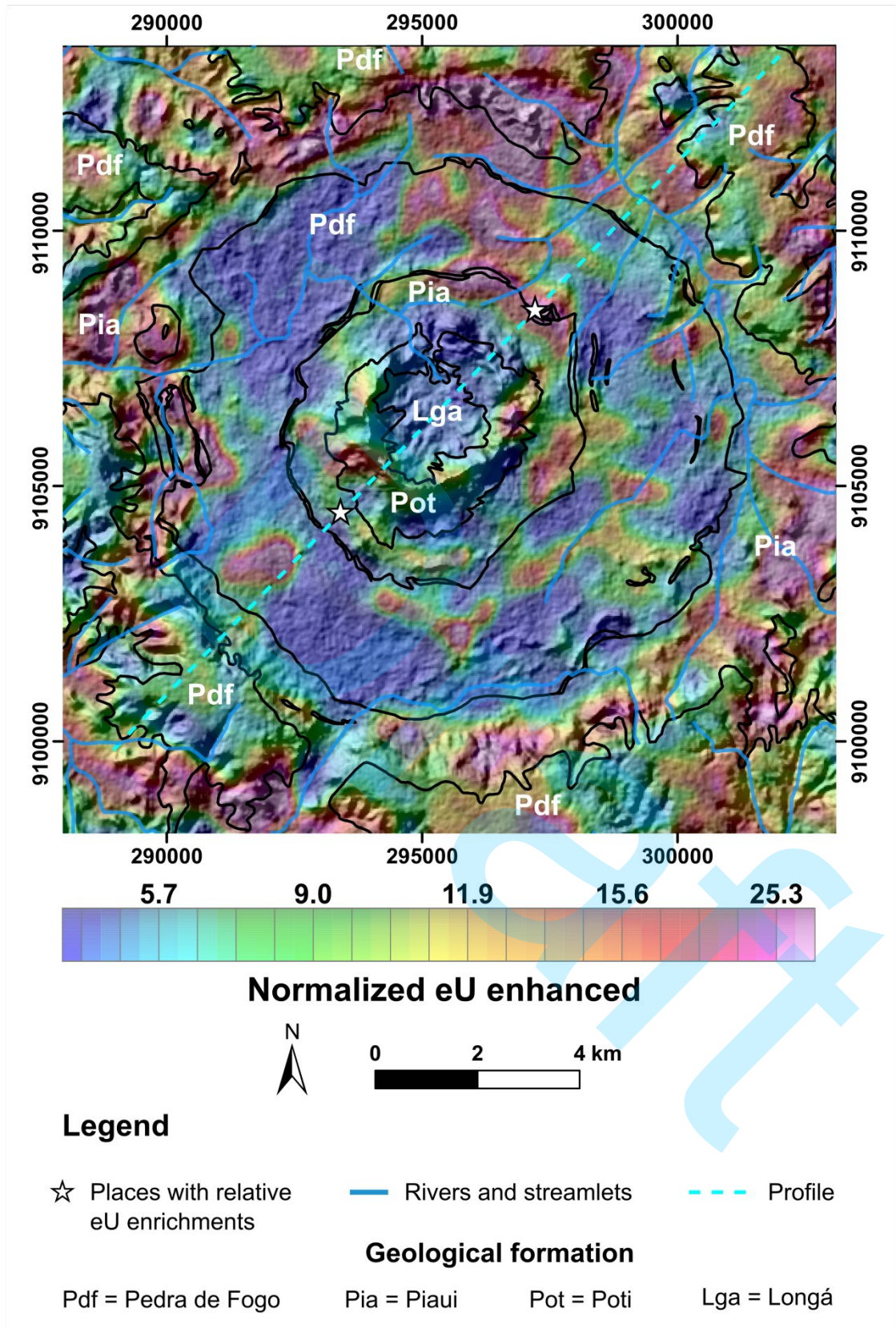
Figure 12: Normalized eU enhancement image (NeU_E) map of Serra da Cangalha impact structure. The white stars highlight areas where eU is relatively enriched compared to K and eTh, in the inner zone of the annular basin.

Other interesting results derived from radiometric maps in Figure 11 concern mapping of Pedra de Fogo Formation. In the eU Inverse Image (Fig. 11), Pedra de Fogo Formation is seen as reddish purple areas whose contours match well those on the geological map as proposed in previous work (Kenkmann et al., 2011; Vasconcelos et al., 2013). Moreover, the central portion of SdC shows yellowish hues, which suggests that the Poti, Piaui, and mainly Longá, formations can be distinguished from the Pedra de Fogo Formation based on eU and eU/K content.

Finally, the outer zone of the SdC structure is well marked by increases of values on the eTh and eU concentration curves (Fig. 10). Both curves then decrease again into the surrounding terrain (outer domain). Abundances of K are low both on the crater rim and over the outer terrain. Increases along the eTh/K and eU/K ratio curves reveal that eTh and eU are relatively enriched with respect to K, whereas a decrease in the eU/eTh curve suggests that eTh is more enriched than eU (Fig. 10). Several studies have reported that such a behavior of radioelements could be due to weathering processes that promote eTh and eU concentration in Fe oxides or their adsorption by phyllosilicate minerals – coincident with leaching of K from weathered soils (e.g., Megumi and Mamuro 1977; Taylor et al. 2002; Wilford and Minty 2007; Mello et al., 2021). Vasconcelos et al. (2012) suggested that the source of eTh and eU could be Fe-oxide minerals in lateritic crusts that formed in soils of the outer rim. Potassium, in contrast, may have been leached from the profile. Abundances of eTh may be relatively increased more than abundances of eU, because the latter radioelement could become leached under oxidizing conditions (Langmuir, 1978; Reinhardt and Hermann, 2018).

CONCLUSIONS

This work presents a synthesis of the Tocantins State Aerogeophysical Atlas, with special emphasis on the interpretation of the first vertical derivative of anomalous magnetic field (FVD – AMF) and RGB color composition of K, eTh, and eU concentration maps. In addition, a special focus was placed onto the aerogeophysical characteristics of the Serra da Cangalha impact structure. Based on visual analysis and previous geological information, we can conclude the following:

Radiometric and/or magnetic signatures of specific geological units (e.g., Mosquito Formation basalts, or granite/gneiss/migmatite terrains), of structural features (e.g. dykes and lineaments), or of related exogenous factors (Serra Geral do Tocantins quartz soils and alluvial deposits on main drainage channels) can be visualized on regional scale magnetic anomaly maps.

The K and eTh Inverse Images prove to be useful tools for highlighting K-rich Natividade – Cavalcante rocks, weathering products in residual landforms, and extents of drainage channels. In the Serra da Cangalha structure, an eU Inverse Image was suitable to outline the Pedra de Fogo Formation contours. Moreover, a normalized eU enhancement map can be a good alternative to map high eU concentrations in the case of SdC.

Analysis of radiometric ratios over the area of the Serra da Cangalha impact structure has provided new insights, mainly regarding the eU concentrations present in the annular basin. Our preferred interpretation suggests that these eU concentrations could be associated with some lithological unit containing U-bearing minerals (e.g., zircon from aeolian sandstone). Alternatively, eU concentrations could also be related to intermittent U anomalies that come from Rn in groundwater discharge zones.

For specific areas, such as the Piauí Formation and the Pedra de Fogo Formation contact zones, eU concentrations may be related to unrecognized mechanisms. For example, notable eU concentrations could stem from brecciated chert layers or silicified sandstones.

We propose that further research about the radiometric signatures of the Serra da Cangalha impact structure is required, and we recommend that a set of data derived from gamma-ray ground surveys, soil sampling, and petrographic descriptions be taken and analyzed by multivariate data analysis techniques.

Declaration of interests

The authors declare that they do not have any known competing financial interests or personal relationships that could have appeared to influence the work reported in this paper.

REFERENCES

Abdallah, S. and Meneghini, P.F.V., 2017, Geologia e Recursos Minerais da Folha Arraias – SD.23 – V – A: Final Report, CPRM, Goiânia, Brazil, 212 pp. Available online at: https://rigeo.cprm.gov.br/handle/doc/17783 (accessed on 05 May 2023).

Airo, M.L, 2002, Aeromagnetic and Aeroradiometric Response to Hydrothermal Alteration: Surveys in Geophysics 23: 273 – 302. DOI: 10.1023/A:1015556614694

Almeida, F.F.M., Hasui, Y., Brito Neves, B.B., and Fuck, R.A., 1981, Brazilian Structural Provinces: An introduction: Earth – Science Reviews 17: 1 – 29. DOI: 10.1016/0012-8252(81)90003-9

Alvarenga, C.J.S., Botelho, N.F., Dardenne, M.A., Lima, O.N.B., and Machado, M.A., 2007, Nota Explicativa das Folhas Monte Alegre de Goiás (SD.23 – V – C – III), Cavalcante (SD.23 – V – C – V) e Nova Roma (SD.23 – V – C – VI). Escala 1:100.000: Final Report, Universidade de Brasília/Companhia de Pesquisa de Recursos Minerais: Goiás, Brazil, 67 pp. Available online at: https://rigeo.cprm.gov.br/handle/doc/18324 (accessed on 05 May 2023).

Alves, P.V.F.S., Botelho, N.F., Dantas, E.L., Cuadros, F.A., 2019, The Cambrian peraluminous Santa Luzia granite suite in the Araguaia Belt, central Brazil: Evidence for closure of the Clymene Ocean based zircon and monazite U – Pb data: Journal of South American Earth Science, 92: 116 – 133. DOI: 10.1016/j.jsames.2019.03.007

Alves, F.M., Silva, E.R., Silva, A.B., 2022, Atlas Aerogeofísico do Estado de Goiás: Serviço Geológico do Brasil – CPRM, Goiânia, 68 pp. Available online at: https://rigeo.sgb.gov.br/handle/doc/23325 (accessed on 07 November 2023).

Arcanjo, S.H.S., Abreu, F.A.M., and Moura C.A.V., 2001, Magmatismo Alcalino Mesoproterozóico na Província Tocantins – Uma Evidência de Quebramento do Supercontinente Rodínia? In: SBG, Simp. Geol. Amazônia, 7.

Arcanjo, S.H.S., Abreu, F.A.M., and Moura, C.A.V., 2013, Evolução geológica das sequências do embasamento do Cinturão Araguaia na região de Alto Paraíso do Tocantins (TO): Brazil: Brazilian Journal of Geology 43 (3): 501 – 514. DOI: http://dx.doi.org/10.5327/Z2317-48892013000300007

Baratoux, D., Niang, C.A.B., Reimold, W.U., Sapah, M.S., Jessell, W., Boamah, D., Faye G., Bouley, S., Vanderhaeghe, O., 2019, Bosumtwi impact structure, Ghana: Evidence for fluidized emplacement of the ejecta: Meteoritics & Planetary Science 54 (10): 2541 - 2556. DOI: 10.1111/maps.13253

Barros, L.D., and Gorayeb, P.S.S., 2019, Serra do Tapa Ophiolite Suite – Araguaia Belt: Geological characterization and Neoproterozoic Evolution (central – northern Brazil): Journal of South American Earth Sciences 96: 102323.DOI: 10.1016/j.jsames.2019.102323

Bierwirth, P., 1996, Investigation of airborne gamma – ray images as a rapid mapping tool for soil and land degradation – Wagga Wagga, NSW. Australian Geological Survey Organisation: Canberra, Australia, 69 pp. Available online at:

https://d28rz98at9flks.cloudfront.net/14903/Rec1996_022.pdf (accessed on 05 May 2023).

Brito Neves, B. B., and Cordani, U. G., 1991, Tectonic Evolution of South America during the Late Proterozoic: Precambrian Research 53 (1 - 2): 23-40, DOI: 10.1016/0301-9268(91)90004-T

Brito Neves, B. B., Fuck, R. A., and Pimentel, M. M, 2014, The Brasiliano collage in South America: a review: Brazilian Journal of Geology 44(3): 493-518. DOI: 10.5327/Z2317-4889201400030010.

Campos, J.E.G. and Dardenne M.A., 1997a, Estratigrafia e sedimentação da Bacia Sanfranciscana: Uma revisão: Revista Brasileira de Geociências 27(3): 269 – 282. Available online at: https://www.ppegeo.igc.usp.br/index.php/rbg/article/view/11291 (accessed on 05 May 2023).

Campos, J.E.G. and Dardenne, M.A., 1997b, Origem e evolução tectônica da Bacia Sanfranciscana: Revista Brasileira de Geociências 27 (3): 283 – 294. Available online at: https://www.ppegeo.igc.usp.br/index.php/rbg/article/view/11293 (accessed on 05 May 2023).

Cheesman, S., MacLeod, I. and Hollyer, G., 1998, A new, rapid, automated grid stitching algorithm: Exploration Geophysics 29(3–4): 301–305. 10.1071/EG998301

Clark, D.A., 1997, Magnetic petrophysics and magnetic petrology: Aids to geological interpretation of magnetic surveys: Journal of Australian Geological and Geophysical 17(2): 83 - 103. Available online at: https://d28rz98at9flks.cloudfront.net/81495/Jou1997_v17_n2_p083.pdf (accessed on 05 May 2023).

CPRM - SERVIÇO GEOLÓGICO DO BRASIL, 2006, Projeto Aerogeofísico Tocantins: relatório final do levantamento e processamento dos dados magnetométricos e gamaespectométricos: São Paulo, SP, Brazil: AeroGeoPhysica LatinoAmericana - AGP-LA. 479 pp. Available online at: https://rigeo.sgb.gov.br/handle/doc/10698 (accessed on 31 October 2023).

CPRM - SERVIÇO GEOLÓGICO DO BRASIL, 2007, Projeto aerogeofísico complemento do Tocantins: relatório final do levantamento e processamento dos dados magnetométricos e gamaespectrométricos: Rio de Janeiro, RJ, Brazil: Lasa Engenharia e Prospecções.Programa Geologia do Brasil – PGB, 124 pp. Available online at: https://rigeo.sgb.gov.br/handle/doc/10227 (accessed on 31 October 2023).

CPRM - SERVIÇO GEOLÓGICO DO BRASIL, 2012, Projeto Aerogeofísico Conceição do Araguaia: relatório final do levantamento e processamento dos dados magnetométricos e gamaespectrométricos: Rio de Janeiro, RJ, Brazil: Lasa Prospecções; Prospectors Aerolevantamentos e Sistemas, Programa Geologia do Brasil – PGB, 296 pp. Available online at: https://rigeo.sgb.gov.br/handle/doc/11454 (accessed on 31 October 2023).

CPRM - SERVIÇO GEOLÓGICO DO BRASIL, 2014, Projeto aerogeofísico Rio Formoso: relatório final do levantamento e processamento dos dados magnetométricos e gamaespectrométricos: Rio de Janeiro, RJ, Brazil: Lasa Prospecções, Programa Geologia do Brasil – PGB, 182 pp. Available online at: https://rigeo.sgb.gov.br/handle/doc/21697 (accessed on 31 October 2023).

CPRM - SERVIÇO GEOLÓGICO DO BRASIL, 2015, Projeto aerogeofísico Rio Maria: relatório final do levantamento e processamento dos dados magnetométricos e gamaespectrométricos: Rio de Janeiro, RJ, Brazil:Prospectors Aerolevantamentos e Sistemas, Programa Geologia do Brasil – PGB, 264 pp. Available online at: https://rigeo.sgb.gov.br/handle/doc/21701. (accessed on 31 October 2023).

Cordani, U.G., Pimentel, M.M., Araújo, C.E.G, Basei, M.A.S, Fuck, R.A., and Girardi, V.A.V., 2013, Was there an Ediacaran Clymene Ocean in central Brazil?: American Journal of Sciences 313: 517-539. DOI: 10.2475/06.2013.01

Crósta, A. P., Reimold, W. U., Vasconcelos, M. A. R., Hausen, N., Oliveira, G. J. G., Maziviero, M. V., and Góes, A. M., 2019, Impact cratering structures: The South American record – Part 1: Geochemistry 79 (1):1 - 61. DOI: 10.1016/j.chemer.2018.06.001.

Cruz, D.J.N. and Gorayeb, P.S.S., 2020, Geology and petrology of the mafic dike swarms of the Araguaia Belt: Evidence

for distinct events of intracontinental magmatism in central – northern Brazil and correlation with large igneous provinces: Journal of South American Earth Sciences 100: 102563. DOI: 10.1016/j.jsames.2020.102563

Dardenne, M. A., 2000, The Brasilia Fold Belt: In: Cordani, U.G., Milani, E.J., Thomaz Filho, A., and Campos, D.A., (eds.), Tectonic Evolution of South America: 31st International Geological Congress: Rio de Janeiro, Brazil, p. 231-263. Available online at: https://rigeo.cprm.gov.br/handle/doc/19419 (accessed on 05 May 2023).

Delgado, I. M., Souza, J. D., Silveira Filho, N. C., Santos, R. A., Pedreira, A. J., Guimarães, J. T., Angelim, L. A A., Vasconcelos, A. M., Gomes, I. P., Lacerda Filho, J. V., Valente, C. R.; Perrota, M. M., Heineck, C. A., 2003, Geotectônica do Escudo Atlântico. In: Bizzi, L. A., Schobbenhaus, C., Vidotti, R. M., and Gonçalves, J. H., (eds.), Geologia, Tectônica e Recursos Minerais do Brasil: Textos, Mapas e GIS. Scale 1:2. 500. 000: CPRM, Brasília, Brazil: 227 - 334. Available online at: https://rigeo. cprm. gov. br/handle/doc/5006 (accessed on 05 May 2023).

Dent, D.L., MacMillan, R.A., Mayr, T., Chapman, W.K., and Berch, S.M., 2013, Use of airborne gamma radiometrics to infer soil properties for a forested area in British Columbia, Canada: Journal of Ecosystem and Management 14 (1): 1 – 12. DOI: 10.22230/jem.2013v14n1a201

Dentith, M. and Mudge, S., 2014, Geophysics for the mineral exploration geoscientist: 1sted., Cambridge University Press: Cambridge, 516 pp. DOI: 10.1017/CBO9781139024358

Dickson, B.L., Scott, K.M, 1997, Interpretation of aerial gamma-ray surveys adding the geochemical factors: Journal of Australian Geology & Geophysics 17 (2): 187 – 200.

Dietz, R. S. and French, B. M., 1973, Two probable astroblemes in Brazil: Nature 244: 561 - 562. 10.1038/244561a0

Duval, J.S., 1983, Composite color images of aerial gamma-ray spectrometric data: Geophysics 48(6): 722-735. 10.1190/1.1441502

Figueiredo, A.J.A., Olimpío, J., and Olivatti, O., 2001., Conceição do Araguaia – Folha SB.22 – X – B, Estado do Tocantins e Pará. Escala 1:250.000, Final Report: CPRM/DIEDIG/DEPAT: Brasília, Brazil, 143 pp. Available online at: https://rigeo.cprm.gov.br/handle/doc/5363 (accessed on 05 May 2023).

Ford, K., Harris, J. R., Shives, R., Carson, J., and Buckle, J., 2008, Remote Predictive Mapping 2. Gamma-Ray Spectrometry: A Tool for Mapping Canada's North: Geoscience Canada 35(3-4): Retrieved from https://journals.lib.unb.ca/index.php/GC/article/view/11270.

Frasca, A.A.S., Lima H.A.F., Moraes, L.L., and Ribeiro, P.S.E, 2010, Geologia e recursos minerais da Folha Gurupi – SC.22 – Z – D. Estado do Tocantins. Scale 1:250.000, Final Report: CPRM: Goiânia, Brazil, 180 pp. Available online at: https://rigeo.cprm.gov.br/handle/doc/10907 (accessed on 05 May 2023).

Frasca, A.A.S., 2015, Amálgamas do W-Gondwana na Província Tocantins: PhD Thesis, Universidade de Brasília - UnB, Brasília, DF, Brazil, 172 pp. Available online at: https://rigeo.cprm.gov.br/handle/doc/15296 (accessed on 05 May 2023).

Frasca, A.A.S., Ribeiro, P.S.E. Lacerda Filho, J.V., Meneghini, P.F.V., Moraes, L.L., and Lima, H.A.F., 2018, Geologia e recursos minerais da Folha Alvorada – SC.22 – X – B. Estado do Tocantins. Escala 1:250.000, Final Report: CPRM: Goiânia, Brazil, 292 pp. Available online at: https://rigeo.cprm.gov.br/handle/doc/20465 (accessed on 05 May 2023).

Fuck, R. A., 1994, A faixa Brasília e a compartimentação Tectônica na Província Tocantins: In: 4th Simpósio de Geologia do Centro - Oeste, SBG: Brasília, Brazil. p. 184-187.

Fuck, R.A., Dantas, E.L., Pimentel, M.M., Botelho N.F., Armstrong R., Laux J.R., Junges S.L., Soares J.E., and Praxedes I.F., 2014, Paleoproterozoic crust-formation and reworking events in the Tocantins Province, Central Brazil: A contribution for Atlantica supercontinent reconstruction: Precambrian Research 244: 53 – 74. DOI: 10.1016/j.precamres.2013.12.003

Galbraith, J.H. and Saunders, D.F., 1983, Rock classification by characteristics of aerial gamma-ray measurements:

.

Journal of Geochemical Exploration 18:49 – 73. DOI: 10.1016/0375-6742(83)90080-8

Gilder, S.A., Pohl, J., Eitel, M, 2018, Magnetic signatures of terrestrial meteorite impact craters: A summary: In: Lühr, H., Wicht, J., Gilder, S.A., Holschneider, M. (eds) (eds), Magnetic Fields in the Solar System: Astrophysics and Space Science Library 448: 357 - 382. DOI: 10.1007/978-3-319-64292-5_13

Góes A.M.O. and Feijó F.J, 1994, Bacia do Parnaíba: Boletim de Geociências da Petrobras 8(1): 57 – 67.

Graça, M.C., Silva, G.F., 2020, Atlas Aerogeofísico do Estado de Rondônia: Serviço Geológico do Brasil – CPRM, Porto Velho, Rondônia, 64 pp. Available online at: https://rigeo.sgb.gov.br/handle/doc/21823 (accessed on 07 November 2023).

Gorayeb, P.S.S., 1981, Evolução geológica da região de Araguacema - Pequizeiro, Goiás: MSc Thesis, Universidade Federal do Pará, Belém, Brazil. 99 pp.

Gunn, P. J., 1997, Regional magnetic and gravity responses of extensional sedimentary basins: Journal of Australian Geology & Geophysics 17(2): 115–131. Available online at: https://d28rz98at9flks.cloudfront.net/81497/Jou1997_v17_n2_p115.pdf (accessed on 05 May 2023).

Hasui, Y., Tassinari, C.C.G., Siga Junior, O., Teixeira, W., Almeida, F.F.M., and Kawashita, K, 1980, Datações Rb-Sr e K-Ar do Centro-Norte do Brasil e seu significado geológico-geotectônico: In 31st Congresso Brasileiro de Geologia, Balneário de Camburiú - SC.

Henkel, H. and Guzmán, M., 1977, Magnetic features of fracture zones: Geoexploration 15(3): 173-181. DOI: 10.1016/0016-7142(77)90024-2

Herz, N., Hasui, Y., Costa, J.B.S., and Matta, M.A.S., 1989, The Araguaia fold belt, Brazil: A reactivated Brasiliano – Pan – African cycle (550 Ma) geosuture: Precambrian Research 42: 371 – 386. DOI: 10.1016/0301-9268(89)90020-X

Hodel, F., Trindade, R.I.F., Macouin, M., Meira, V.T., Dantas, E.L., Paixão, M.A.P., Rospabé, M., Castro, M.P., Queiroga, G.N., Alkmin, A.R., and Lana, C.C., 2018, A Neoproterozoic hyper-extended margin associated with Rodinia's demise and Gondwana's build-up: The Araguaia Belt, central Brazil: Gondwana Research 66: 43 - 62. DOI: 10.1016/j.gr.2018.08.010

International Atomic Energy Agency (IAEA), 2003, Guidelines for radioelement mapping using gamma-ray spectrometry data. IAEA, Vienna, Austria, 179 pp.

Johnson, A., Cheeseman, S. and Ferris, J., 1999, Improved compilation of Antarctic Peninsula magnetic data by new interactive grid suturing and blending methods: Annali Di Geofisica 42(2), 249–259. 10.4401/ag-3717

Jost, H., Chemale Jr, F., Dissin, I. A., and Tassinari, C. C. G., 2010, Goiás greenstone belts: Archean or Paleoproterozoic: In: 45th CONGRESSO BRASILEIRO DE GEOLOGIA, SGB, São Paulo, p. PAP33.

Jost, H.; Chemale Jr., F.; Fuck, R. A., Dussin, I. A., 2013, Uvá complex, the oldest orthogneisses of the Archean-Paleoproterozoic terrane of central Brazil: Journal of South American Earth Sciences 47: 201 - 212. DOI: 10.1016/j.jsames.2013.07.002

Kenkmann, T., Vasconcelos, M. A. R., Crósta, A. P., Reimold, W. U., 2011, The complex impact structure Serra da Cangalha, Tocantins State, Brazil: Meteoritics & Planetary Science 46 (6): 875 – 889. DOI: 10.1111/j.1945-5100.2011.01199.x

Langmuir, D, 1978, Uranium solution-mineral equilibria at low temperatures with applications to sedimentary ore deposits: Geochimica et Cosmochimica Acta 42 (6A): 547-569. DOI: 10.1016/0016-7037(78)90001-7

Leite E.P., Lambert J., Vasconcelos M.A.R., Crósta A.P. and Batezelli A., 2022, Gamma-ray spectrometry of the Araguainha impact structure, Brazil: Additional insights into element mobilization due to hydrothermal alteration:

Anais da Academia Brasileira de Ciências 94(3): 1 - 16. 10.1590/0001-3765202220210182

Li, X., 2006, Understanding 3D analytical signal amplitude: Geophysics 71(2): L13- L16. 10.1190/1.2184367

Li, Y. and Nabighian, M., 2015, Tools and Techniques: Magnetic Methods of Exploration – Principles and Algorithms. In: Schubert G., Treatise on Geophysics, 2nd ed., Elsevier: 335 - 391. 10.1016/B978-0-444-53802-4.00196-2.

Maia de Souza, C. S., Hauser, N., Dantas, E. L., Reimold, W. U., Schmitt, R. T., Chaves, J. G. S., and Osorio, L. F. B., 2019, Does the metavolcanic-sedimentary Rio do Coco Group, Araguaia Belt, Brazil, represent a continuity of the Quatipuru ophiolitic complex? – Constraints from U-Pb and Sm-Nd isotope data: Journal of South American Earth Sciences 94, 102233. 10.1016/j.jsames.2019.102233.

Mantovani, M.S.M. and Brito Neves, B.B., 2009, The Paranapanema lithospheric block: its nature and role in the accretion of Gondwana: In: Gaucher C., Sial, A.N., Halverson, G.P., Frimmel H.E. (eds.), Neoproterozoic Cambrian Tectonics, Global Change and Evolution: a focus on southwestern Gondwana: Developments in Precambrian Geology, 16: 257–272. DOI: 10.1016/S0166-2635(09)01619-3

Marques, R.P., Kassab Jr F., Molina E.C., Andrade F.A.R. (org.), 2006, Levantamentos aerogeofísicos para a identificação de áreas com ocorrência potencial de petróleo e gás na Bacia do Parnaíba – Tomo II: área Parnaíba – Aerolevantamento magnético e gamaespectrométrico, Final Report, São Paulo, v. I.A, Convênio ANP – USP, 109 pp.

Marini, O. J., Fuck,, R. A., Danni, J. C. M., Dardenne, M. A., Loghercio, S. O. C., and Ramalho, R., 1984, As faixas de dobramentos Brasília, Uruaçu e Paraguai-Araguaia e o Maciço mediano de Goiás. In: Schobbenhaus, C., Campos, D. A., Derze, G. R., Asmus, H. E: Geologia do Brasil, DNPM, Brasília, Brazil: 251-303.

Marini, O. J.; Botelho, N. F. A., 1986, Província de Granitos Estaníferos de Goiás: Revista da Sociedade Brasileira de Geociências 16 (4): 119 - 131. Available online at: http://www.ppegeo.igc.usp.br/index.php/rbg/article/view/12029 (accessed on 05 May 2023).

Maziviero, M. V., Vasconcelos, M. A., Crósta, A. P., Góes, A. M., Reimold, W. U., and De C. Carneiro, C., 2013, Geology and impact features of Riachão structure, northern Brazil: Meteoritics & Planetary Science 48(10): 2044-2058. DOI: 10.1111/maps.12213

Martins-Ferreira, M.A.C., Chemale, F., Dias, A.N.C., and Campos, J.E.G., 2018a, Proterozoic intracontinental basin succession in the western margin of the São Francisco Craton: Constraints from detrital zircon geochronology: Journal of South American Earth Sciences 81: 165 - 176. DOI: 10.1016/j.jsames.2017.11.018.

Martins-Ferreira, M.A.C., Campos, J.E.G., Von Huelsen, M.G., and Neri, B.L., 2018b, Paleorift structure constrained by gravity and stratigraphic data: The Statherian Araí rift case: Tectonophysics 738 – 739: 64 - 82. DOI: 10.1016/j.tecto.2018.05.014.

Martins-Ferreira, M.C., Dias, A.N.C., Chemale, F., Campos, J.E.G., Seraine, M., and Rodrigues, E.N. 2020, Multi–stage crustal accretion by magmatic flare-up and quiescence intervals in the western margin of the São Francisco Craton: U – Pb – Hf and geochemical constraints from the Almas Terrane: Gondwana Research 85: 32 - 54. DOI: 10.1016/j.gr.2020.04.005

Martins-Neto, M.A., Pedrosa-Soares, A.C., and Lima, S.A.A., 2001, Tectono – sedimentary evolution of sedimentary basins from Late Paleoproterozoic to Late Neoproterozoic in the São Francisco craton and Araçuai fold belt, eastern Brazil: Sedimentary Geology 141 – 142: 343 – 370. DOI: 10.1016/S0037-0738(01)00082-3

Martins-Neto, M.A., 2009, Sequence stratigraphic framework of Proterozoic successions in eastern Brazil: Marine and Petroleum Geology 26: 163–176. DOI: 10.1016/j.marpetgeo.2007.10.001

Megumi, K. and Mamuro, T., 1977, Concentration of uranium series nuclides in soil particles in relation to their size: Journal of Geophysical Research 10(2): 353-356. DOI: 10.1029/JB082i002p00353

.

Mello, D.C., Demattê, J.A.M., Oliveira Mello, F.A., Poppiel, R.R., Silveiro, N.E.Q., Safanelli, J.L., Barros e Sousa, A., Di Raimo, L.A.L., Rizzo, R., Resende, M.E.B. and Schaefer, C.E.G.R., 2021, Applied gamma – ray spectrometry for evaluating tropical soil processes and attributes: Geoderma 381: 114736. DOI: 10.1016/j.geoderma.2020.114736

Milligan, P. R. and Gunn, P. J., 1997, Enhancement and presentation of airborne geophysical data: AGSO Journal of Australian Geology and Geophysics 17(2): 63-75. Available online at: https://dev.ecat.ga.gov.au/geonetwork/srv/api/records/fae9173a-71b2-71e4-e044-00144fdd4fa6 (accessed on 05 May 2023).

Minty, B., 2011, Short note: on the use of radioelement ratios to enhance gamma-ray spectrometric data: Exploration Geophysics 42(1): 116-120. DOI: 10.1071/EG10011.

Mocitaiba, L.S.R., Castro, D.L., and Oliveira, D.C., 2017, Cartografia geofísica regional do magmatismo mesocenozóico na Bacia do Parnaíba: Geologia USP - Série Científica 17(2): 169-192. 10.11606/issn.2316-9095.v17-455

Moura, C.A.V., Gaudette, H.E., 1999, Zircon ages of basement orthogneisses from the northern segment of the Araguaia Belt, Brazil: In: Sinha, A.K. (ed). Basement Tectonics 13: 155 – 178. DOI: 10.1007/978-94-011-4800-9_10

Nabighian M. N., 1972, The analytical signal of two-dimensional magnetic bodies with polygonal cross-section: its properties and use for automated anomaly interpretation: Geophysics 37(3): 507-517. 10.1190/1.1440276

Niang, C.A.B., Baratoux, D., Diallo, D.P., Rochette, P., Jessell, M.W., Reimold, W.U., Bouley, S., Vanderhaeghe, O., Faye, G., Lambert, P., 2021, Systematic survey of K, Th, and U signatures in airborne radiometric data from Australian meteorite impact structures: Possible causes of circular features and implications: In: Reimold W.U., Koeberl C. (eds). Large Meteorite Impacts and Planetary Evolution VI: Geological Society of America, Special Paper 550: 373 - 405. DOI: 10.1130/2021.2550(15).

Niang C.A.B., Baratoux, D., Rochette, P., Braucher, R., Reimold, W.U., Lambert, P., Diallo, D.P., Regard, V., Carretier, S., Jessell, M.W., Faye, G., Koeberl, C., 2022, The origin of the potassium-rich annular zones at the Bosumtwi impact structure, Ghana, investigated by field study, radiometric analysis, and first cosmogenic nuclide data: Meteoritics & Planetary Science 57(3): 702–729. DOI: 10.1111/maps.13788

O´Leary, D., Brown, C. and Daly, E., 2022, Digital soil mapping of peatland using airborne radiometric data and supervised machine learning - Implication for assessment of carbon stock: Geoderma 428: 116086. 1 - 15. 10.1016/j.geoderma.2022.116086

Oliveira, I.W.B., 2000, Zinco, chumbo e cobre de Palmeirópolis – Estado do Tocantins: Informe de Recursos Minerais, 10, CPRM: Goiânia, Brazil, 22 pp.

Oliveira, A.L., Pimentel, M.M., Fuck, R.A., and Oliveira, D.C., 2018, Petrology of Jurassic and Cretaceous basaltic formations from the Parnaíba Basin, NE Brazil: correlations and associations with large igneous provinces: In: Daly, M.C., Fuck, R.A., Julià, F., MacDonald, I.M., and Watts A.B (eds). Cratonic basin formation: a case study of the Parnaíba Basin of Brazil: Geological Society, London, Special Publication 472: 279 – 308. DOI: 10.6084/m9.figshare.c.3985437.

Oliveira, R.G., Rodrigues, M.A.C. 2019. Atlas Aerogeofísico do Estado de Pernambuco: Serviço Geológico do Brasil – CPRM, Recife, Pernambuco, Brazil. p. 66. Available online at: https://rigeo.cprm.gov.br/handle/doc/21419 (accessed on 05 May 2023).

Oliveira, V.S. 2022. Atlas Aerogeofísico do Estado de Roraima: Serviço Geológico do Brasil – CPRM, Manaus, Amazonas, p. 106. Available online at: https://rigeo.sgb.gov.br/handle/doc/22788 (accessed on 05 May 2023).

Paixão, M. A. P., Nilson, A. A., and Dantas, E. L., 2008, The Neoproterozoic Quatipuru ophiolite and the Araguaia fold belt, central-northern Brazil, compared with correlatives in NW Africa: In: Pankhurst, R. J., Trouw, R. A. J., Brito Neves, B. B., and Wit, M. J.. (eds). West Gondwana: Pre-Cenozoic Correlations Across the South Atlantic Region. Bath, UK: The Geological Society Publishing House 294: 297-318. DOI: 10.1144/SP294.16

Pickup, G. and Marks, A., 2000, Identifying large – scale erosion and deposition process from airborne gamma radiometrics and digital elevation models in a weathered landscape: Earth Surface Processes and Landforms 25: 535 – 557. DOI: 10.1002/(SICI)1096-9837(200005)25:5<535::AID-ESP91>3.0.CO;2-N

Pilkington, M., and Grieve, R. A. F., 1992, The geophysical signature of terrestrial impact craters: Reviews of Geophysics 30(2): 161-181.

Pimentel, M.M. and Fuck R.A., 1992, Neoproterozoic crustal accretion in central Brazil: Geology 20: 375–379. DOI: 10.1130/0091-7613(1992)020<0375:NCAICB>2.3.CO;2

Pimentel, M. M., Fuck, R. A., and Gioia, S. M. C. L., 2000, The Neoproterozoic Goiás Magmatic Arc, central Brazil: a review and new Sm-Nd data: Revista Brasileira de Geociências 30 (1): 35-39. Available online at: https://ppegeo.igc.usp.br/index.php/rbg/article/view/10866 (accessed on 05 May 2023).

Pinto, L.G.R., 2022.Levantamentos aerogeofísicos no Serviço Geológico do Brasil - Histórico, Produtos e Futuro: In: IX Simpósio Brasileiro de Geofísica, SBGf, Curitiba, PR, Brazil. Available online at: https://sbgf.org.br/mysbgf/resumos_expandidos.php?page=1&evento=IX_SimBGf&session=Geof%C3%ADsica%20Aplicada%20%C3%A0%20Cartografia%20Geol%C3%B3gica&sort=sessionarticle (accessed on 16 Nov 2023)

Pires de Lima, R. and Marfurt, K. J., 2018, Principal component analysis and K-means analysis of airborne gamma-ray spectrometry surveys: 88th Annual International Meeting, SEG, Expanded Abstracts: 2277–2281, doi: 10.1190/segam2018-2996506.1

Ramos V.A., Vujovich G., Martino R., Otamendi J. 2010. Pampia: a large cratonic block missing in the Rodinia Supercontinent: Journal of Geodynamics 50:243-255. DOI: 10.1016/j.jog.2010.01.019

Rawlins, B.G. and Webster, R, 2007, Understanding airborne radiometric survey signals across part of eastern England: Earth Surface Processes and Landforms 32: 1503 – 1515. DOI: 10.1002/esp.1468

Reeves C, 2005, Aeromagnetic Surveys: Principles, Practice & Interpretation: Washington DC, Geosoft, 155, Ch. 6: 6–18.

Reid, A., 2012, Forgotten truths, myths and sacred cows of Potential Fields Geophysics – II: SEG Technical Program Expanded Abstracts : 1-3.10.1190/SEGAM2012-0178.1

Reinhardt, N. and Hermann, L. 2018, Gamma–ray spectrometry as a versatile tool in soil Science: A critical review: J. Plant Nutr. Soil Sci. 182 (1): 1 -19. DOI: 10.1002/jpln.201700447

Reimold, W.U., Cooper, G.R.J., Romano, R., Cowan, D.R., and Koeberl C., 2006, Investigation of Shuttle Radar Topography Mission data of the possible impact structure at Serra da Cangalha, Brazil: Meteoritics & Planetary Science 41(2): 237-246. DOI: 10.1111/j.1945-5100.2006.tb00207.x

Ribeiro, P.S.E. and Alves C.L., 2017, Geologia e recursos minerais da região de Palmas – Folhas Miracema do Norte SC.22 – X – D, Porto Nacional SC.22 – Z – B e Santa Teresinha SC.22 – Z – A, Escala 1:250.000: Final Report, CPRM: Goiânia, Brazil, 485 p. Available online at: https://rigeo.cprm.gov.br/handle/doc/18076 (accessed on 05 May 2023)

Ribeiro, P.S.E., Frasca, A.A.S., Carneiro, J.S.M., Hattingh K., Rezende, E.S., Martins, F.R., 2022, Mapa geológico e de recursos minerais do Estado do Tocantins, Escala 1:500.000: Maps and GIS files, CPRM, Goiânia, Brazil. Available online at: https://rigeo.sgb.gov.br/handle/doc/22530 (accessed on 26 October 2023)

Roest, W.R., Verhoef, J. and Pilkington, M., 1992, Magnetic interpretation using the 3–D analytic signal: Geophysics 57: 116–125. 10.1190/1.1443174

Sabóia, A.M. and Meneghini, P.F.V, 2019, Geologia e Recursos Minerais da Folha Dianópolis – SC.23 – Y – C, Escala 1:250.000: Final Report, CPRM, Goiânia, Brazil, 193 p. Available online at: https://rigeo.cprm.gov.br/handle/doc/17734 (accessed on 05 May 2023)

Santos, J.O.S, 2003, Geotectônica dos Escudos das Guianas e Brasil-Central: In: Bizzi, L.A., Schobbenhaus, C., Vidotti, R.M., Gonçalves, J.H., Geologia, Tectônica e Recursos Minerais do Brasil: CPRM, Brasília, Brazil: 169 - 226.

Schobbenhaus C., Ribeiro C.L., Oliva L.A., Takanohashi J.T., Lindenmayer A.G., Vasconcelos J.C., and Orlandi V, 1975, Folha Goiás (SC-22) Carta Geológica do Brasil ao Milionésimo. Texto Explicativo. DNPM, Brasília, Brazil, p. 99-113.

Sgarbi, G.N.C., Sgarbi, P.B.A., Campos, J.E.G., Dardenne, M.A., and Penha, U.C, 2001, Bacia Sanfranciscana: O Registro Fanerozóico da Bacia do São Francisco: In: Pinto, C.P., Martins-Neto M.A. (eds), Bacia do São Francisco: Geologia e Recursos Naturais: SBG-MG, Belo Horizonte, Brazil: 93 – 138.

Silva, A.B. and Alves, F.M, 2021, Atlas Aerogeofísico do Estado do Tocantins: Serviço Geológico do Brasil – CPRM, Goiânia, Goiás, 87 pp. Available online at: https://rigeo.cprm.gov.br/handle/doc/22566 (accessed on 05 May 2023)

Silva, A., and Alves, F.M., 2022, Understanding the Origin of the Airborne Geophysical Signatures of the Jalapão Geomorphological Units, Urucuia Basin, Central–Northern Brazil: Journal of the Geological Survey of Brazil 5(3): 205-20. DOI: 10.29396/jgsb.2022.v5.n3.4.

Soares, J.E.P., Stephenson, R., Fuck, R.A., Lima, M.V.A.G., Araújo, V.C.M., Lima, F.T., Rocha, F.A.S., and Trindade, C.R., 2018, Structure of the crust and upper mantle beneath the Parnaíba Basin, Brazil, from wide-angle reflection data: In: Daly, M.C., Fuck, R.A., Julià, J., MacDonald, D.I.M., and Watts, A.B. (eds) Cratonic Basin Formation: A case study of the Parnaíba Basin of Brazil: Geological Society, London, Special Publication, 472. DOI: 10.1144/SP472.9

Sousa, P.A.B., Borges, R.S.T., Dias, R.R.. 2012. Atlas do Tocantins: subsídios ao planejamento da gestão territorial, Diretoria de Zoneamento ecológico (DZE), Departamento de Pesquisa e Zoneamento Ecológico – Econômico: SEPLAN, Palmas, TO, Brazil, 80 pp.

Sousa, F.R.F.O., 2021. Atlas Aerogeofísico do Estado do Ceará. Serviço Geológico do Brasil – CPRM, Fortaleza, Ceará, 100 pp.. Available online at: https://rigeo.sgb.gov.br/handle/doc/22449 (accessed on 07 November 2023).

Spadoni, M. and Voltaggio, M., 2013, Contribution of gamma ground spectrometry to the textural characterization and mapping of floodplain sediments: Journal of Geochemical Exploration 125: 20 – 33. DOI: 10.1016/j.gexplo.2012.10.016

Taylor, M.J., Smettem, K., Pracillo, G., and Verboom, W., 2002, Relationships between soil properties and high resolution radiometrics, central eastern Wheatbelt, Western Australia: Exploration Geophysics 33: 95–102. DOI: 10.1071/EG02095.

Vasconcelos, M. A. R., Leite, E. P., and Crósta, A. P., 2012, Contributions of gamma-ray spectrometry to terrestrial impact crater studies: The example of Serra da Cangalha, northeastern Brazil: Geophysical Research Letters 39 (4): L04306. DOI: 10.1029/2011GL050525.

Vasconcelos, M. A. R., Crósta, A. P., Reimold, W.U., Góes, A. M., Kenkmann, T., and Poelchau, M. H., 2013, The Serra da Cangalha impact structure, Brazil: Geological, stratigraphic and petrographic aspects of a recently confirmed impact structure: Journal of South American Earth Sciences 45: 316-330, DOI: 10.1016/j.jsames.2013.03.007.

Vaz, P.T., Rezende, N.G.A.M., Wanderley, Filho J.R., and Travassos, W.A.S., 2007, Bacia do Parnaíba: Boletim de Geociências da Petrobras 15 (2): 253–263.

Wilford, J., Minty, B., 2007, The use of airborne gamma-ray imagery for mapping soils and understanding landscape processes: In: Legacherie, P., McBratney, A.B., and Voltz, M. (eds), Developments in Soil Science 31: Ch. 16, 207 – 218. DOI: 10.1016/S0166-2481(06)31016-1